EVALUATION OF SOLITARY WAVES AS A MECHANISM FOR OIL TRANSPORT IN ELASTIC POROUS MEDIA: A CASE STUDY OF THE SOUTH EUGENE ISLAND FIELD, GULF OF MEXICO BASIN

A Thesis

presented to

the Faculty of the Graduate School

at the University of Missouri-Columbia

In Partial Fulfillment

of the Requirements for the Degree

Master of Science

---

by

AJIT JOSHI

Dr. Martin Appold, Thesis Supervisor

MAY 2012

The undersigned, appointed by the dean of the Graduate School, have examined the thesis entitled

EVALUATION OF SOLITARY WAVES AS A MECHANISM FOR OIL TRANSPORT IN ELASTIC POROUS MEDIA: A CASE STUDY OF THE SOUTH EUGENE ISLAND FIELD, GULF OF MEXICO BASIN

presented by Ajit Joshi,

a candidate for the degree of Master of Science,

and hereby certify that, in their opinion, it is worthy of acceptance.

Professor Martin Appold

Professor Mian Liu

Professor Sergei Kopeikin

……dedicated to my loving parents.

ACKNOWLEDGEMENTS

I would like to acknowledge and express my sincere gratitude to several people who helped me, encouraged me and motivated me during my graduate program at this university. First and foremost, I am very indebted to my advisor, Dr. Martin Appold, whose support, encouragement, motivation and generous co-operation from the very beginning resulted in the successful completion of this thesis work. I am very much thankful to my thesis committee members, Dr. Mian Liu and Dr. Sergei Kopeikin, for their time to be in my thesis committee and to provide feedbacks, comments and suggestions to improve this thesis. It is my pleasure to thank Dr. Jeffrey Nunn from the Department of Geology and Geophysics at Louisiana State University for his input to this research.

Moreover, I would like to thank the entire faculty, staff and my colleagues in the MU Department of Geological Sciences for their help, guidance and support that encouraged me and provided me an excellent environment to conduct my research. I would also like to acknowledge and show gratitude to the US Department of Energy for funding this research under grant DE-FG02-08ER15958. Lastly, I would be very grateful to my loving parents who consistently encouraged me in my study without letting me know any of their difficulties.

TABLE OF CONTENTS

LIST OF FIGURES

LIST OF TABLES

Table Page

ABSTRACT

Hydrocarbons in shallow (< 1 km depth) Pleistocene sand reservoirs of the Eugene Island 330 field in the northern Gulf of Mexico basin are thought to have originated from Early Tertiary source sediments at depths of about 4.5 km. Despite the low permeability of the intervening sediments, hydrocarbons appear to have moved rapidly through these sediments, which are hypothesized to have occurred as solitary waves, i.e. discrete pressure pulses, along the Red growth fault system. The purpose of the present research was to evaluate the mechanics of solitary wave formation and movement during sedimentation, diagenesis, and source rock maturation in the Eugene Island hydrocarbon field. A detailed two-dimensional model coupling sedimentation, compaction, hydrocarbon generation, heat transport, and multi-phase fluid flow predicted overpressures of 52 MPa by the present day in the hydrocarbon source sediments, with most of the overpressure caused by compaction disequilibrium and the remainder by hydrocarbon generation. Movement along the Red growth fault was rapid enough to cause a pressure decrease of several MPa from the upthrown block to the downthrown block, consistent with field observations. The average pressure generation rate at the base of the Red fault during the period of hydrocarbon formation was predicted to be about 10^{-6} Pa/s. Based on the likely values of fault permeability and the calculated magnitude of the pressure gradients generated by the compaction-dominated flow regime, flow velocities on the order of 10^{-6} m/Myr would be expected, which is far too low for hydrocarbons to ascend kilometer-scale distances and accumulate in shallow Pleistocene reservoirs within the 3.6 million year lifespan of the minibasin.

To evaluate solitary wave behavior, a separate one-dimensional model was constructed that used the pressure generation rate determined from the two-dimensional basin model and solved the continuity equation for a single fluid phase consisting of oil using an implicit finite difference method over a five kilometer vertical profile. The calculations showed that solitary waves were only able to form and migrate over a narrow permeability range of about 10^{-25} to 10^{-24} m^2. Within this permeability range, solitary waves could reach velocities on the order of 10^{-3} m/yr. For permeabilities greater than 10^{-24} m^2, fluid pressures diffuse too rapidly from the source region for a coherent wave to form. For permeabilities lower than 10^{-25} m^2, the solitary wave grows to large amplitude but is effectively immobile over million year time scales. Solitary wave formation and propagation required high initial fluid pressures in the range of about 91-93% of lithostatic pressure. When fluid pressure lay outside of this range, then because of the sensitivity of permeability to effective stress, permeability lay outside of the 10^{-25} to 10^{-24} m^2 range such that solitary waves either did not form or formed but did not move significantly from their source location. As solitary waves ascend, their velocity increases while their amplitude diminishes and they leave behind a wake of slightly elevated fluid pressures (typically 1-2 MPa above the initial background values) that increases the permeability enough to prevent further solitary waves from forming. Thus, for time spans on the order of the 3.6 million year history of Eugene Island, solitary waves would not form in succession, which limits their hydrocarbon transport efficacy. Solitary waves were only able to ascend 1-2 kilometers from their source regions before their amplitudes diminished to background fluid pressure and porosity values. As they

ascend their velocity increases from order 0.1 mm/year to order 1 mm/year. Wave volume was found to increase during the early stages of ascent, peaking after a travel distance of about 0.5 to 1 km at a pore volume of about order 10^5 m^3. Thus, solitary waves are unlikely to have charged the shallow Pleistocene reservoirs at Eugene Island with oil, though it is possible that solitary waves could be important agents of oil transport in other locations where the reservoirs are more proximal to the source rocks.

1. Introduction

Hydrocarbon reservoirs and sources are commonly separated by kilometer-scale thicknesses of low permeability sediments that can be traversed by fluids in remarkably short periods of time (Holland et al, 1990; Whelan et al, 1994; Losh et al, 1999; Revil and Cathles, 2002). For example, in the northern Gulf of Mexico basin, most hydrocarbon production has come from thermally immature Tertiary and Quaternary reservoirs into which the hydrocarbons have migrated from sources typically 2 to 4 km deeper shortly after reservoir deposition and trap formation (Young et al., 1977; Dow, 1984; Curtis, 1991). In the Eugene Island minibasin, historically one of the most productive hydrocarbon fields on the outer continental shelf of the Gulf of Mexico basin, hydrocarbons are concentrated in shallow Pliocene-Pleistocene sand reservoirs but migrated from early Tertiary sediments lying at depths of about 4.5 km. These Tertiary sediments may have been the source of the hydrocarbons (Holland et al., 1990), or alternatively, temporary reservoirs that were originally charged from deeper Jurassic-Cretaceous source sediments (Thompson, 1988, 1991; Whelan et al., 1994). Stratigraphic, structural, and fluid pressure relations indicate that the Pliocene-Pleistocene reservoirs were charged within the past 0.7 million years (Holland et al., 1990; Alexander & Handschy, 1998; Losh et al., 1999), indicating flow rates on the order of at least 10^{-3} m/yr.

However, flow rates could have been much greater than that. For example, Whelan et al. (2001) documented changes in hydrocarbon composition in shallow reservoirs at Eugene Island on the order of several years, which they attributed to

recharge from deeper sources with a sm aller contribution from biodegradation. High fluid flow rates are commonly made possible by the existence of permeable faults, which in the case of Eugene Island appears principally to be the Red Fault, a major growth fault bounding the eastern margin of the minibasin (Figure 1). This is supported by a study by Lin and Nunn (1997), which showed a plum e of low salinity fluid extending along the Red Fault from depth and protruding into shallower reservoirs.

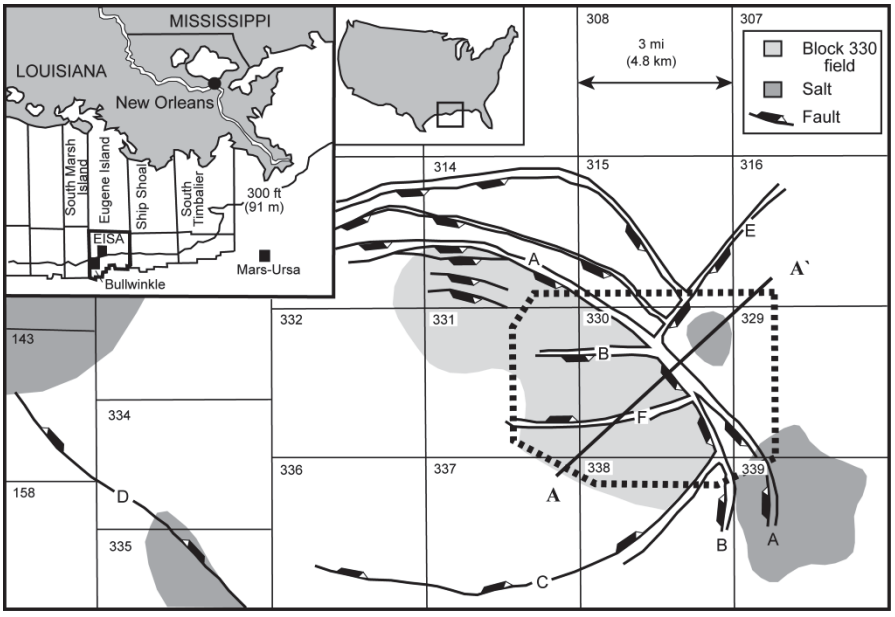

Figure 1. Location map of the Eugene Island 330 minibasin on the continental shelf of offshore Louisiana (Alexander & Flemings, 1995). Line AA' shows the location of the cross-section across a Red fault and antithetic fault (designated as A and F respectively in the figure) used in the two-dimensional model.

A further important observation is that fluid flow in the Red Fault appears to have been transient and episodic rather than steady and continuous. Anderson et al. (1994)

found that the permeability of the Red Fault could be increased sufficiently to admit large-scale fluid flow for fluid pressure increases of at least 3.5 MPa above current values. This led them to suggest a mechanism for fluid flow in which fluid pressure builds at depth over time until a threshold is reached that causes the fault permeability to increase enough to allow a transient burst of fluid flow and fluid pressure release, after which the fault seals and the process repeats. Losh et al. (1999) identified a thermal anomaly centered on the Red Fault based on vitrinite reflectance and carbon and oxygen isotope data. They determined that this anomaly could be explained by the ascent of a short-lived (~150 year-long) pulse of rapidly flowing fluid at a rate of over 300 m/yr that heated the fault zone by as much as 55° C above present-day ambient temperatures. Further support for this mechanism has come from the numerical modeling work of Roberts and Nunn (1995), Guerin (2000), and Roberts (2001), though Guerin's (2000) work suggested longer time scales of flow of 1000 to 5000 years. Revil and Cathles (2002) suggested that these transient episodes of rapid fluid flow could represent solitary waves, manifest as regions of elevated fluid pressure and porosity, and first proposed by Rice (1992) as a mechanism for enhanced fluid transport in fault zones with elastic rheologies. Revil and Cathles (2002) developed an analytical solution to a differential equation for flow through porous media that allowed them to compute velocities of solitary waves. Using values of physical parameters appropriate for Eugene Island, they found solitary wave velocities on the order of at least 1's of km/yr to be possible, with even higher velocities on the order of 100's of km/yr more likely. Four-dimensional seismic reflection data presented by Haney et al. (2005b) may record the ascent of a

solitary wave through the Red fault. The data show a zone of high reflectivity thought to be associated with anomalously high fluid pressure that moved at an average rate of about 140 m/yr.

Other previous studies have also shown that solitary waves can develop and serve as important fluid transport agents in sedimentary porous media. Appold & Nunn (2002) carried out one-dimensional numerical modeling of solitary wave formation and movement in viscous porous media saturated with petroleum and undergoing active compaction and hydrocarbon generation. In this scenario, solitary waves are manifest as regions of elevated liquid fraction (fluid-saturated porosity) that ascend due to buoyancy rather than pressure gradients, and are initiated by increases in liquid fraction caused by the conversion of kerogen in the solid matrix to petroleum. Appold & Nunn (2002) found solitary wave development to be promoted by high sedimentation rate and total organic carbon content and low matrix shear viscosity. Solitary waves did not always provide enhanced petroleum transport relative to conventional Darcian flow, but only when the background porosity was low (less than about 1%).

Bourlange and Henry (2007) used two-dimensional numerical modeling to study solitary wave migration in the Nankai accretionary wedge in which the porous media were assumed to have an elastic rheology. Using a finite element solution to the groundwater flow equation, Bourlange and Henry (2007) showed that overpressure generated at depth along a décollement can diffuse as a discrete plume rapidly updip, provided that the hydraulic diffusivity of the décollement is high in absolute terms as well as relative to the surrounding porous media. However, the pressure surges that they

generated in their models did not have closed wave forms and were not episodic, in contrast to the indications from the empirical field data cited above, or to the results from Appold and Nunn (2002) for viscous porous media.

The aim of the present research was to quantify the behavior of solitary waves in elastic porous media in a sedimentary basinal environment like that of Eugene Island, where high overpressures are produced by compaction, hydrocarbon generation through the maturation of kerogen, or gas generation through cracking of previously formed oil. The specific hypothesis is that solitary waves would be spawned in the Red fault and perhaps other faults where they intersect zones of overpressure. The focus of the research has been in two principal areas: (1) characterizing fluid pressure evolution in the Eugene Island minibasin over the course of its formation; (2) quantifying the size, velocity, and fluid transport capabilities of solitary waves as a function of the properties of the porous medium and pore fluid.

2. Geological Setting of South Eugene Island 330

The geology of the Eugene Island minibasin has been described in several publications, including Holland et al. (1990), Anderson et al. (1991), and Alexander and Flemings (1995), from which the following summary is based. The Eugene Island minibasin is located in the outer continental shelf of the Gulf of Mexico basin, approximately 270 km southwest of New Orleans. The basin is elliptical in shape, with dimensions of about 20×15 kilometers, and is filled with siliciclastic sediments of Pliocene-Pleistocene age. The basin formed as a result of deltaic sediment loading that caused underlying Late Miocene-age salt to flow into adjacent areas. The evacuated salt left a topographic low at the surface that could receive sediments from the advancing delta. The evacuating salt also produced four major fault zones along the boundaries of the basin—normal listric growth faults in the north and northeast and antithetic faults in the south and west. Motion along the growth faults has produced rollover anticlines in the downthrown blocks that have served as the principal traps for hydrocarbons. The hydrocarbons are concentrated in the eastern part of the basin in seven Pleistocene quartzose to slightly arkosic fine-grained sandstone reservoirs. The reservoirs have porosities averaging about 30%, water saturations between 20 and 40%, and permeabilities ranging from 10^{-14} m^2 to more than 6×10^{-12} m^2. Mudstone sealing layers have much lower permeabilities on the order of 10^{-19} m^2 (Stump & Flemings, 2002). Production of hydrocarbons from Eugene Island began in 1972, peaking from 1975-1980 at about 95,000 barrels of oil and 0.482 trillion cubic feet of gas per day, during which time Eugene Island was the most productive hydrocarbon field in the federal outer

continental shelf (Holland et al., 1990).

The structural and stratigraphic evolution of the minibasin has been subdivided into three phases: an early prodelta, an intermediate proximal deltaic, and a late fluvial phase (Figure 2). The prodelta phase is characterized by the deposition of shales, turbidites, and sands upon a Miocene salt sheet. As this deposition progressed, space for additional sedimentation was created by withdrawal of the underlying salt sheet. The Lentic sand is a major reservoir that was deposited during this phase and is strongly overpressured (Alexander and Flemings, 1995). During the proximal deltaic phase, alternating beds of sand and mud were deposited in distributary channel, channel-mouth bar, and delta-front environments. In the Eugene Island literature, the principal sand reservoirs are designated OI, MG, LF, KE, JD, and HB, and are moderately overpressured. During the fluvial phase, little accommodation space for further deposition of sediments was created because by this time the underlying salt had been completely evacuated. This led to a southward progradation of the deltaic system in shallow water. The GA sand was deposited early in this phase when faults in the basin were still active. This active faulting provided structural closure to make the GA a good reservoir, in contrast to the sands that were deposited later. Sediments deposited during the fluvial phase are hydrostatically pressured (Lin and Nunn, 1997).

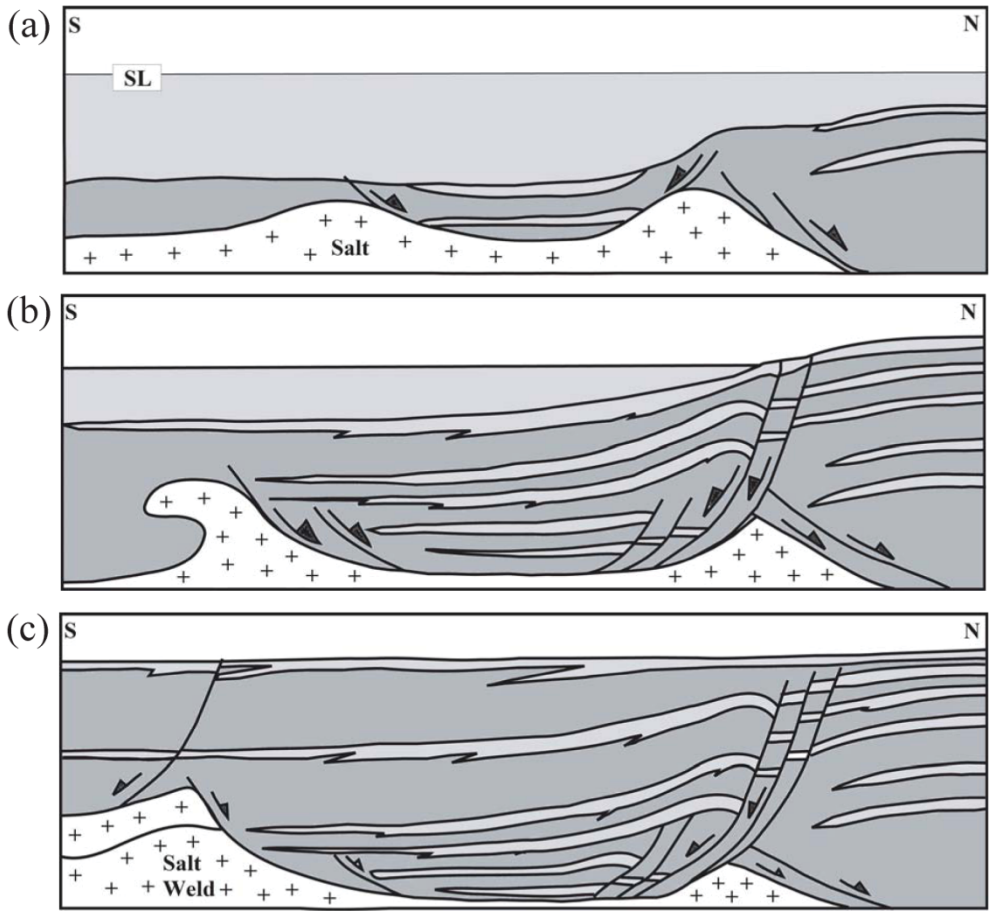

Figure 2. Evolution of the Eugene Island 330 minibasin from prior to 2.8 Ma to the present time showing three phases: (a) prodelta (b) proximal deltaic and (c) fluvial (Alexander & Flemings, 1995).

3. Modeling of Eugene Island Minibasin Evolution

3.1. *Theoretical Background*

In order to determine if overpressures sufficient for the generation of solitary waves could be generated in the Eugene Island minibasin, the evolution of the minibasin from its inception about 3.6 Ma to the present day was modeled using the BasinMod® 2-D software. The model reconstructed the chronologic deposition of the major stratigraphic units, their compaction and heating during burial, the maturation of kerogen and formation of oil and methane in presumed hydrocarbon source sediments, changes in the pore pressure and proportions of water, oil, and methane, and the velocities of their flow.

The model was based on a backstripped cross section of Eugene Island published by Gordon and Flemings (1998). Sedimentation rates were computed from the known ages and thicknesses of the sedimentary units, corrected for compaction as a result of burial using the approach of Sclater and Christie (1980). Fluid pressure as a function of compaction and heat transport as a function of conduction and advection were computed following the theory presented by Bethke (1985), with the addition of saturation-dependent relative permeability and capillary pressure relationships to account for the presence of hydrocarbon fluid phases with water. The formation of hydrocarbons from kerogen was computed using the kinetic model of Sweeney and Burnham (1990) for type II kerogen. Hydrocarbons could begin to flow out of their source media once their pore pressures exceeded threshold capillary pressures. The permeability of each lithologic unit was calculated as a function of its grain size distribution using a modified Kozeny-

Carman equation (Ungerer et al, 1990). These grain size values as well as other key model parameters are shown in Table 1. Further details regarding model construction are described next.

3.2. *Model Construction*

As noted above, the Eugene Island minibasin evolution model for the present study was based on a cross section published by Gordon and Flemings (1998), extended to a depth of 5 km (Fig. 3). The cross section was discretized to form a numerical grid with an average horizontal nodal spacing of 25 m. The vertical nodal spacing was governed by the sedimentation rate and a time step size selected to be 50,000 years.

Several model scenarios were investigated. The first is referred to as the "base case scenario" that employs the most likely parameter values for Eugene Island (Table 1). Parameter values as shown in the table, except for porosity, permeability, heat capacity, matrix thermal conductivity and %TOC were based on the empirical data from Platte River Associates for various lithological units (BasinMod1-D®, 2009; BasinMod2-D®, 2009). Bulk thermal conductivities were calculated assuming a geothermal gradient of 33° C/km (Nunn et al., 1984) and a basal heat flux of 60 mW/m^2. Thermal conductivities for shales and sandstones lie in the range from 1 to 3 and 2 to 4 W m^{-1} $K^{-}1$ respectively (Anderson et al, 1991). Heat capacities for each of the lithological units were based on the data by Robie et al. (1979). Most of the sand reservoirs in the Eugene Island minibasin have permeabilities that range from 10^{-12} m^2 to 10^{-13} m^2 and porosities that average about 30% (Holland et al., 1980). Shales are thought to have much lower permeabilities in the range of 10^{-17} m^2 at shallower depths to as low as 10^{-25} m^2 at greater

depths (Matthai & Roberts, 1996; Gordon and Flemings, 1998; Guerin, 2000; Roberts, 2001; Revil & Cathles, 2002). In addition, model scenarios were computed in which the permeabilities of the stratigraphic units were all increased by a factor of 10, 100, and 1000, and in which the permeabilities of the stratigraphic units with the exception of the lower shale were all decreased by a factor of 10 relative to the base case scenario. These alternate scenarios were intended to test the sensitivity of the predicted fluid pressure evolution to uncertainties in permeability values.

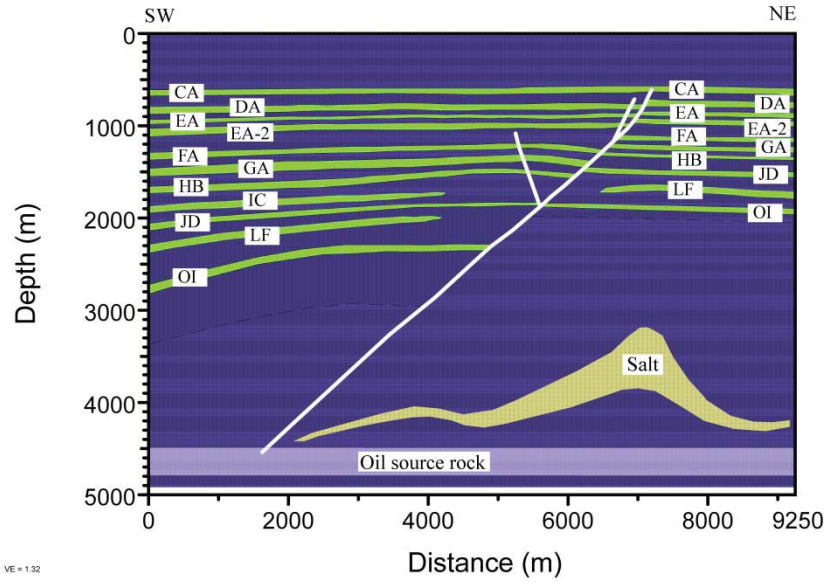

Figure 3. Model cross-section of the Eugene Island minibasin along a northeast to southwest transect shown in Figure 1 (modified from Gordon and Flemings, 1998). Labeled light green layers represent sand reservoirs and purple indicates shale. The light purple layer at the bottom of the cross section represents a kerogen-rich source rock for oil and gas. The bold white lines represents the Red fault system. The yellow patterned region represents salt. The dashed line below the OI sand represents transgressive Lentic 1 surface described by Alexander and Flemings (1995).

The following boundary conditions were applied in all of the models. The bottom of the model domain was considered to be a no-flow boundary based on the compacted nature of the sediments and the possible presence of a salt sill at 5 km depth (Whelan et al., 1994; Revil and Cathles, 2002). The bottom boundary was also assigned a constant heat flux of 60 mW/m^2 (Anderson et al., 1991; Guerin, 2000). The lateral boundaries of the problem domain were insulating with respect to heat flow but were open with respect to fluid flow with pressure specified to be hydrostatic. The upper boundary of the model domain had a constant temperature specified to be 5° C and pressure specified to be hydrostatic.

All of the models considered hydrocarbons to have been sourced from Early Tertiary sediments over a present-day depth interval of about 4.5 to 4.8 km. Shallower Pleistocene shales that are interbedded with Pleistocene sand reservoirs were probably not good sources for hydrocarbons because of their thermal immaturity and low organic carbon content (TOC 0.30-0.80%; Holland et al, 1980). The models assumed the Tertiary source sediments to contain Type II kerogen with a total organic carbon content of 5%. Holland et al (1990) suggested that maturation of source rock and oil generation in the Eugene Island 330 fields occurred at depths of 4570 to 4880 m based on a variety of biomarkers and maturity indicators, which was the approximate source rock depth interval used in the models. The Pleistocene shales in the models were assigned an average organic carbon content of 0.55%.

3.3. Results

As noted above, the purpose of the basin modeling was to characterize the

evolution of pore pressure at Eugene Island, with a particular focus on the rate of fluid pressure increase that could be expected in the hydrocarbon source sedim ents near the Red fault. These predicted rates served as an im portant input for the solitary wave generation and propagation calculations and are fundamental to the evaluation of whether or not solitary waves could serve as a mechanism for enhanced hydrocarbon transport.

The simulation results for the base case scenario are shown in Figures 4-8. Figure 4 shows the stratigraphic evolution of the basin at 3.0 Ma, 2.5 Ma, 1.5 Ma, 1.0 Ma, 0.5 Ma and 0 Ma. Sedimentation in the basin began before 3.0 Ma with the deposition of shale, a source rock for oil and gas, followed by a major salt layer . Continued sedimentation in the basin between 2.5 and 1.5 Ma resulted in the for mation of the Red fault. Growth of the fault ceased in the model after 0.5 Ma by which time salt evacuation and the production of further accommodation space for sedim entation is thought to have ceased (Alexander and Flemings, 1995). The principal hydrocarbon reservoirs were deposited alternately with shale layers between 1.5 Ma and 0.5 Ma. Sedim entation in the model concluded with the deposition of a layer of shale from 0.5 to 0 Ma.

Figure 5 shows a plot of excess pore fluid pressure (i.e. overpressure) as a function of time. Pore fluid pressure remains near hydrostatic levels throughout the basin until about 3.0 Ma. By 2.5 Ma, excess pressure s of about 21 MPa have developed in the lower part of the basin, increasing to abou t 30 MPa by 1.5 Ma. As fluids are drawn toward the newly for med Red fault, a m ajor permeable conduit, fluid pressures are locally reduced around the fault. The package of interbedded sands and shales deposited after 1.5 Ma is overall less compressible than the earlier deposited shales so that much

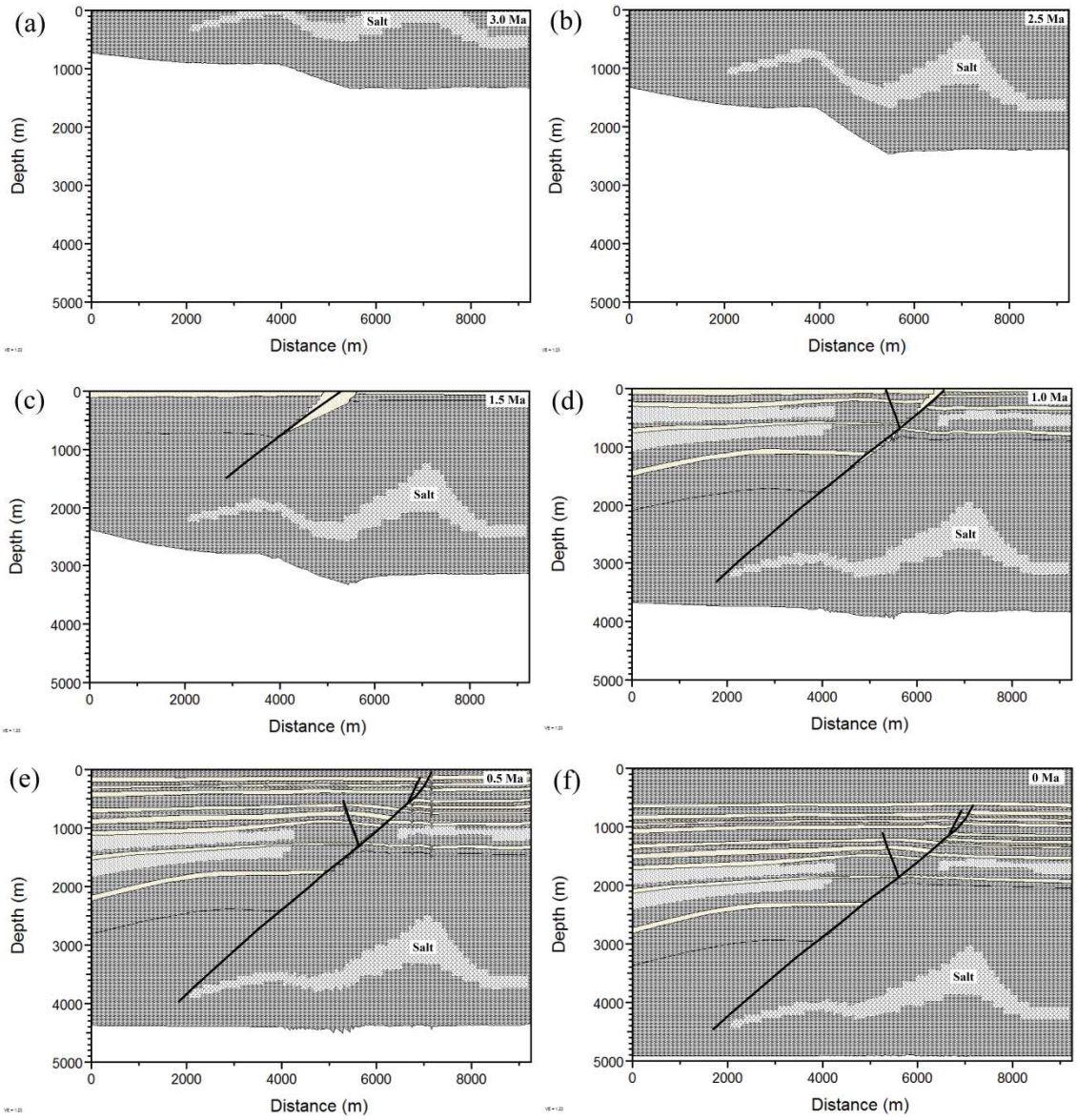

Figure 4. Model stratigraphic evolution of the Eugene Island minibasin at (a) 3.0 Ma, (b) 2.5 Ma, (c) 1.5 Ma, (d) 1.0 Ma, (e) 0.5 Ma, (f) 0 Ma. Light gray and dark gray shades represent sand and shale, respectively. A zone of intermediate gray shading represents salt and is labeled accordingly. White regions around the fault at 1.5 and 1.0 Ma represent stratigraphic gaps created in the model's attempt to render fault offset.

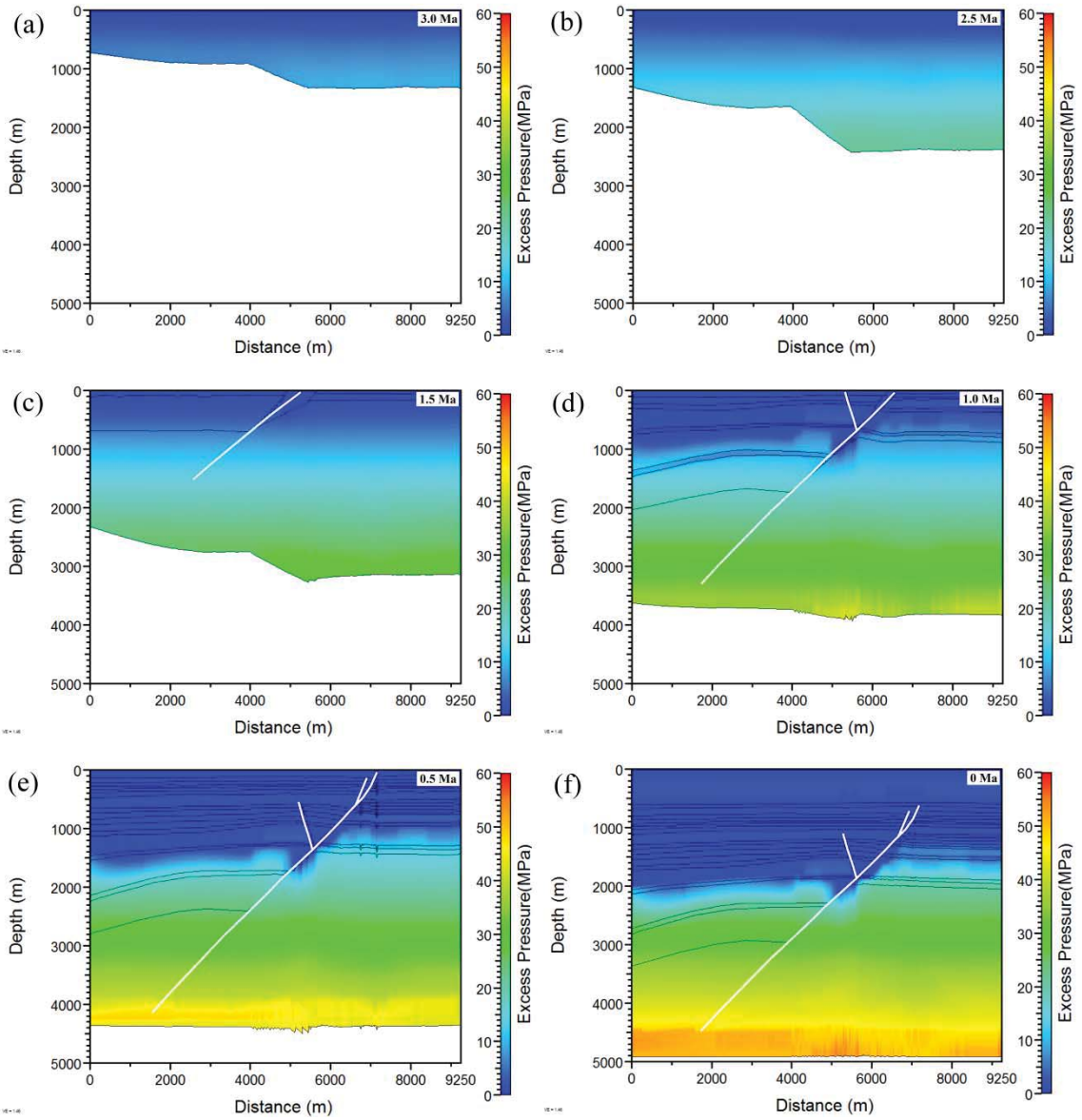

Figure 5. Evolution of excess fluid pressure (i.e. ov erpressure) in the Eugene Island minibasin at (a) 3.0 Ma, (b) 2.5 Ma, (c) 1.5 Ma, (d) 1.0 Ma, (e) 0.5 Ma, (f) 0 Ma for the base case scenario. Thin black lines represent boundaries between stratigraphic units.

less overpressuring develops in the younger sediments than developed in the older shales at comparable depths in their respective burial histories. Fluid pressures in most of these younger sediments remain near hydrostatic throughout the simulations. As the hanging wall side of the fault is displaced downward providing greater accommodation space for further sedimentation compared to the footwall side, overpressured sediments in the downthrown block are advected downward and buried more deeply than sediments on the upthrown block, creating a significant pressure displacement across the fault that has also been observed in the field (Gordon and Flemings, 1998). Overpressures continue to build in the lower shale section, though more slowly over time as the shale becomes more compacted. Excess pressure at the base of the model near the Red fault reaches 35 MPa by 1.0 Ma, 47 MPa by 0.5 Ma, and 52 MPa by the present day. Given the low permeability of 10^{-25} m^2 and the pressure gradients predicted in the lower shale, oil velocities in the lower shale would be no higher than order 10^{-6} m/Myr. Thus, the model predicts that the prevailing fluid flow regime in the Eugene Island minibasin under the base case scenario conditions would have generated flow rates through the lower shale that are about nine orders of magnitude too low to allow kilometer-scale transport of hydrocarbons from source sediments to reservoirs in less than one million years, unless the Red fault served as a much more permeable conduit through the shale.

Figure 6 illustrates the sensitivity of fluid pressure to variations in permeability and compares fluid pressure-depth profiles predicted by the models to the profiles observed in the field near the Red fault in both the upthrown and downthrown blocks. Overall, the base case model prediction compares favorably to the observed field data

(Hart et al., 1995; Revil and Cathles, 2002), which extend to a depth of about 2.5 km. Decreasing permeability by a factor of 10 causes fluid pressures to deviate in the models to significantly higher pressures compared to the field data, especially in the downthrown block. Increasing permeability has a more muted effect, particularly in the upthrown block, leading to decreased fluid pressure relative to the field data. At depths below about 2.5 km in the downthrown block and below about 3.5 km in the upthrown block, the model fluid pressure-depth profiles converge, indicating that fluid pressure in the deeper part of the minibasin is relatively insensitive to the variations in permeability investigated.

The evolution of temperature predicted by the modeling is shown in figure 7. Temperature decreases relatively linearly with depth from 3.0 Ma to 1.5 Ma, due mostly to the effects of conduction. Low temperature anomalies most visible at intermediate depths between 1.5 and 1.0 Ma coincide with a salt layer, whose high thermal conductivity and low heat capacity causes it to lose heat more rapidly than the surrounding sediments. With the development of the Red fault, cooler sediments on the hanging wall side of the fault on the left side of the model domain are advected downward, resulting in a significant temperature displacement across the fault of as much as 40° C by 0.5 Ma. Although fluid flow is enhanced along the fault relative to the surrounding sediments, the enhancement is not great enough to cause a perturbation in temperature along the fault. This conflicts with the findings of Losh et al. (1999), who claimed that temperature along the Red fault had been elevated by as much as 55° C relative to the surroundings. However, this temperature elevation may only have been

transient and could perhaps have been caused by transient, more rapidly moving phenomena like solitary waves, rather than by continuous compaction-driven flow that prevailed over most of the minibasin's history.

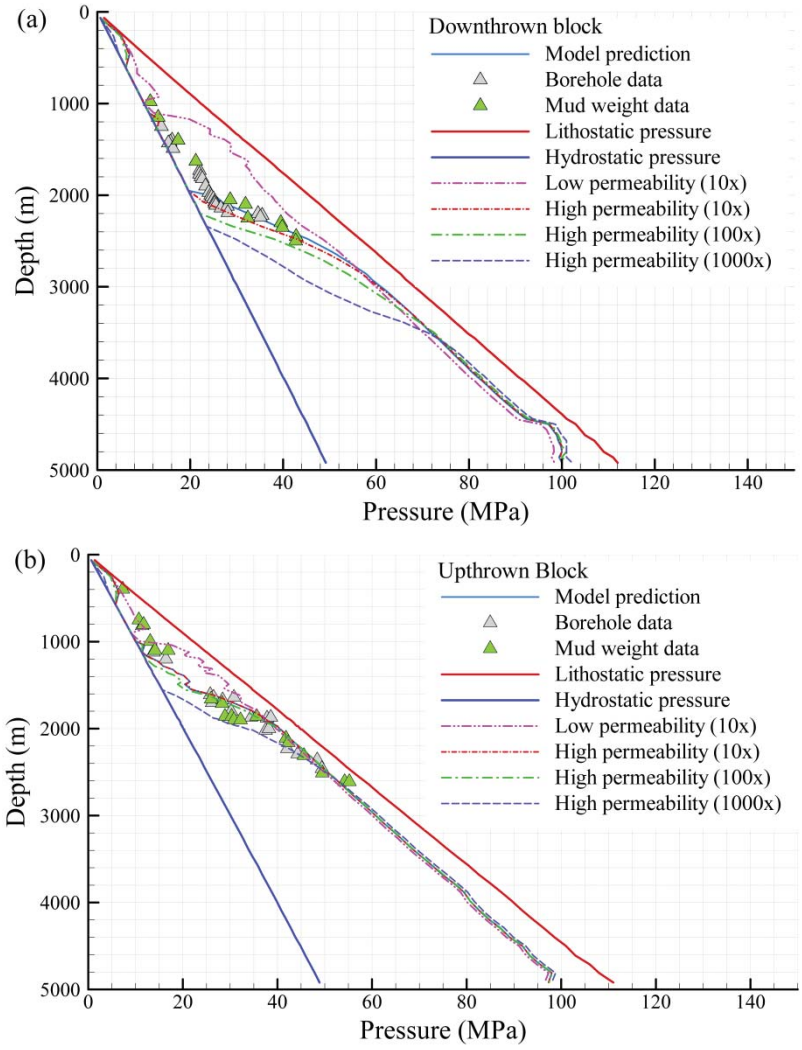

Figure 6. Plots of model (current study) and observed (Revil and Cathles, 2002; Hart et al., 1995) pore pressures as a function of depth for (a) the downthrown side, and (b) the upthrown side of the Red fault in the Eugene Island minibasin for the present day.

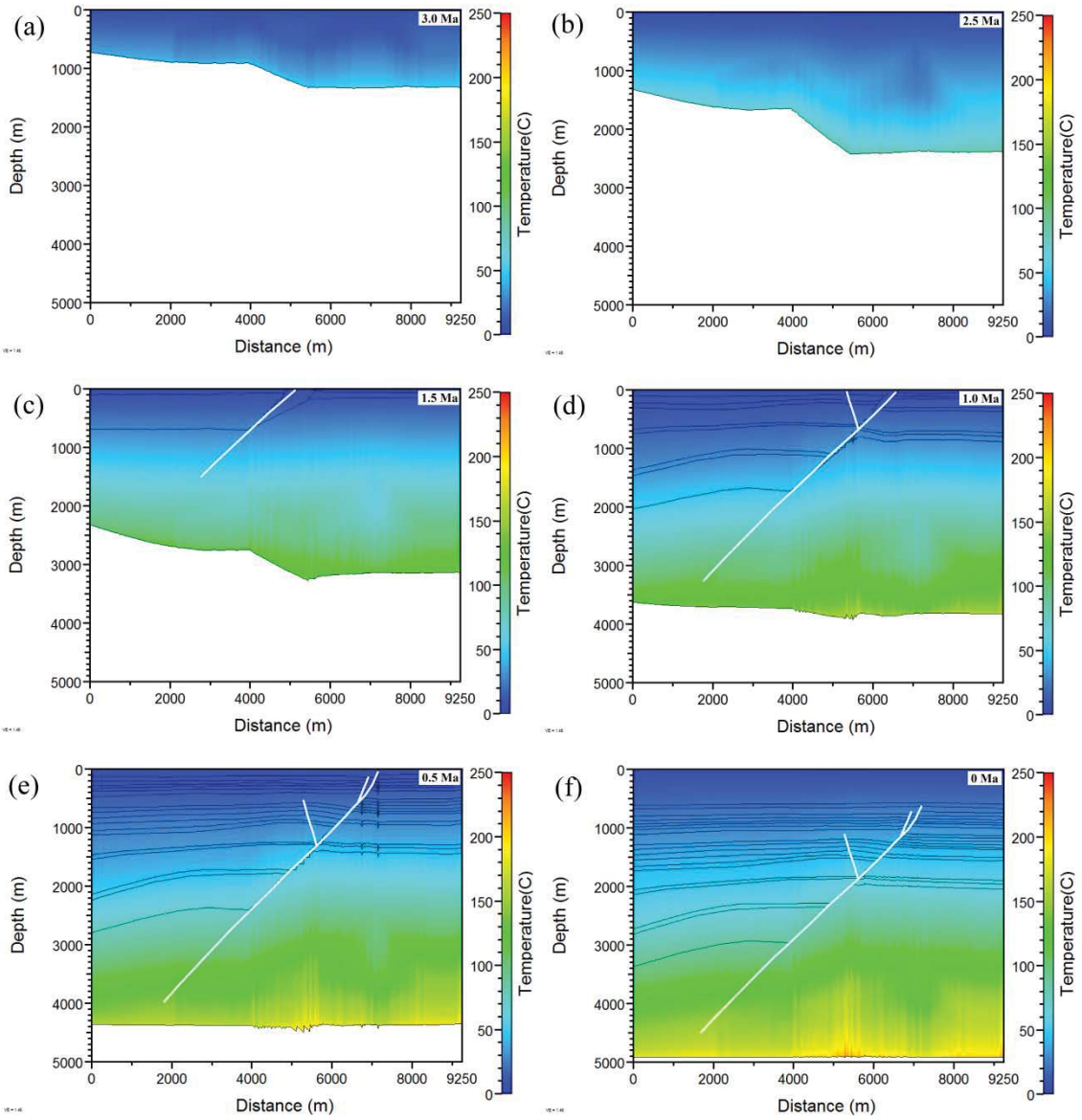

Figure 7. Temperature evolution in the Eugene Island minibasin at (a) 3.0 Ma, (b) 2.5 Ma, (c) 1.5 Ma, (d) 1.0 Ma, (e) 0.5 Ma, (f) 0 Ma for the base case scenario.

The modeling predicts that temperature in the hydrostatically pressured sediments at depths of less than 1.5 km never exceeded 50° C. This indicates that the shales

interbedded with the sand reservoirs never became hot enough to serve as source rocks for the Eugene Island hydrocarbons. However, at the present-day 4.5 to 4.8 km depths suggested by Holland et al. (1990) to have been the source rock interval in the minibasin, temperatures reached 150° C to 170° C, which would have been high enough to generate both oil and gas.

Figure 8 shows the modeled rate of fluid pressure increase over time at the base of the Red fault, including the separate contributions from compaction disequilibrium and hydrocarbon generation. The total fluid pressure generation rate for the first two million years of the simulation varies for the most part between about 3×10^{-7} and 1.5×10^{-6} Pa/s. Thereafter the pressure generation rate is more variable, reaching a maximum value of 2.2×10^{-6} Pa/s at about 1.25 Ma and 1.8×10^{-6} Pa/s at about 0.64 Ma when the contribution from hydrocarbon generation is highest. However, most of the excess fluid pressure at Eugene Island is predicted to come from compaction disequilibrium. This is consistent with the findings of Hart et al. (1995) and Gordon and Flemings (1998), which indicate that compaction disequilibrium accounts for about 75 to 94% of present day overpressure in the minibasin, respectively, with the remainder originating from hydrocarbon generation. Fluid pressure generation from hydrocarbon formation decreases sharply after its peak around 0.64 Ma and reaches negative values after about 0.4 Ma. These negative hydrocarbon pressure generation rates are a result of oil migrating more rapidly out of the source rock than it is being formed.

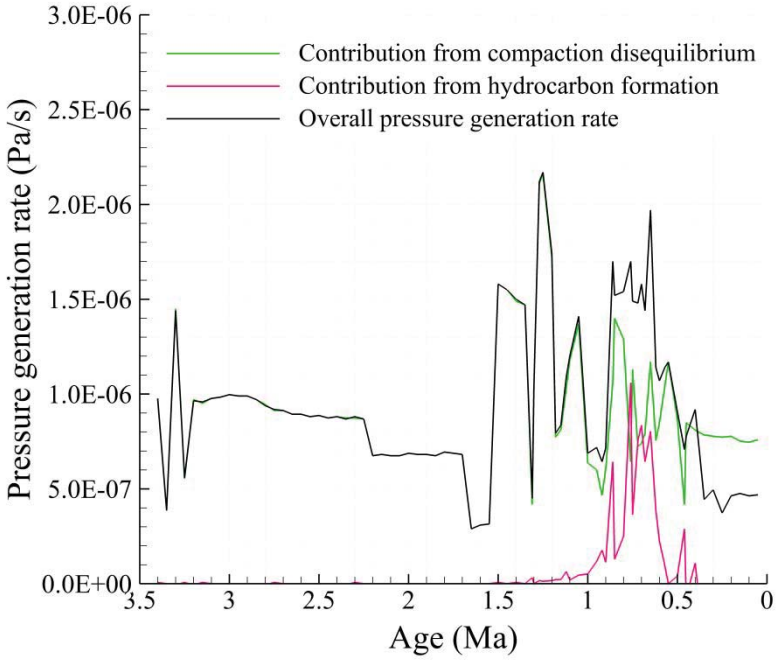

Figure 8. Fluid pressure generation rate over time at the base of the Red fault due to compaction disequilibrium, hydrocarbon generation, and the combined effects of both processes calculated for the base case scenario.

Oil pressure generation rate and temperature were not found to vary significantly in the models within the range of permeabilities tested, and thus plots of these results are not shown. These insensitivities are probably due to the fact that the permeabilities tested were all low enough such that fluid pressure increase due to compaction and heat transport due to conduction were unmodified by the effects of advection.

4. Modeling of Solitary Wave Behavior

Previous research has indicated that solitary waves can arise and propagate in elastic porous media whose permeability increases sharply with decreasing effective stress (Rice, 1992; Revil & Cathles, 2002; Bourlange & Henry, 2007). Furthermore, solitary wave behavior is described by conventional pore fluid pressure diffusion equations that combine mass balance, fluid and matrix constitutive relationships, and Darcy's law. This theory was applied in the present study to investigate solitary wave origin and movement in a one-dimensional vertical profile fully saturated with petroleum representing the Red fault zone. The solitary wave calculations were carried out separately from the Eugene Island minibasin evolution modeling described above, but incorporated the average pressure generation rate predicted by that modeling. The principal governing equations used for the solitary wave calculations are presented next.

4.1. Governing Equations

Equation (1) represents the pore pressure diffusion equation that was used in the present study, which has been modified from the form used by Bourlange and Henry (2007) to include a specific storage term (S_s) more commonly used in hydrogeology (Freeze & Cherry, 1979; Fetter, 2001; Schwartz & Zhang, 2003; Ingebritsen et al., 2006).

$$\frac{d}{dz}\left(\frac{k}{\mu}\left(\frac{dP}{dz}-\rho_f g\right)\right)=\frac{s_S}{\rho_f g}\frac{dP}{dt} \tag{1}$$

Here, k is the permeability of the porous medium, P, μ, and ρ_f represent pore fluid pressure, viscosity, and density, respectively, g is gravitational acceleration, t is time, and

z is the vertical spatial coordinate. This equation was solved assuming that the density of the pore fluid is constant. The dependence of permeability on effective stress is described by (Revil and Cathles, 2002):

$$k = k_0 e^{-\sigma_e/\sigma^*} \tag{2}$$

where k_0 is the permeability at zero ef fective stress, σ^* is an empirical parameter that represents the influence of com paction on perm eability, and σ_e is the effective stress. The specific storage of the porous m edium, S_s, is a function of the com pressibility of the porous medium and of the pore fluid, and is expressed by

$$S_s = \rho_f g(\beta_b + \phi\beta_f) \tag{3}$$

where β_b is the com pressibility of the porous m edium, ϕ is porosity, and β_f is the compressibility of the pore fluid. Porosity at Eugene Island was found to depend on effective stress according to the following equation (Gordon & Flemings, 1998)

$$\phi = \phi_0 e^{-\beta_b \sigma_e} \tag{4}$$

where ϕ_0 is the porosity at a depth of zero. Petroleum viscosity was allowed to vary with temperature and was calculated using the following relation obtained from Middleton and Wilcock (1994),

$$\mu = (1.663 \times 10^6) T^{-3.368} \tag{5}$$

where T is the tem perature of the pore fluid. The background Darcy velocity wa s calculated as a function of pore pressure g radient using the variable-density form of Darcy's law,

$$q = -\frac{k}{\mu}\left(\frac{dP}{dz} - \rho_f g\right) \tag{6}$$

4.2. Model Construction

Solitary wave behavior was investigated by solving equations (1)-(6) over a five kilometer vertical profile saturated with oil representing the Red fault zone using an implicit finite difference method for equation (1) with constant nodal spacing. Four different scenarios were investigated (Table 2): (1) a base-case scenario, (2) an "optimized" scenario that employed model parameter values within geologically reasonable ranges that optimized solitary wave formation and migration, (3) a "high permeability" scenario, and (4) a "low permeability" scenario. In all of the model scenarios, the initial pore fluid pressure distribution was assigned according to the equation,

$$P = X\rho_b g d \tag{7}$$

where X is a fraction that was set to 0.93 in the base case, high and low permeability scenarios, and to 0.95 in the optimized scenario, ρ_b is the density of the bulk porous medium, and d is depth, with pressure at depths of zero and five kilometers remaining constant over time as Dirichlet boundary conditions. The density of the bulk porous medium was calculated from

$$\rho_b = \phi\rho_f + (1-\phi)\rho_g \tag{8}$$

where ρ_g represents the density of the solid mineral grains. The initial permeability profile was calculated using equation (2), where the effective stress was calculated from

$$\sigma_e = \sigma_T - P \tag{9}$$

where σ_T represents total stress. The total stress could be calculated from equation (7) by letting $\sigma_T = P$ and setting $X = 1$. The initial permeability profiles for the four model

scenarios are shown in Figure 9, and the parameter values used to generate them are shown in Table 2.

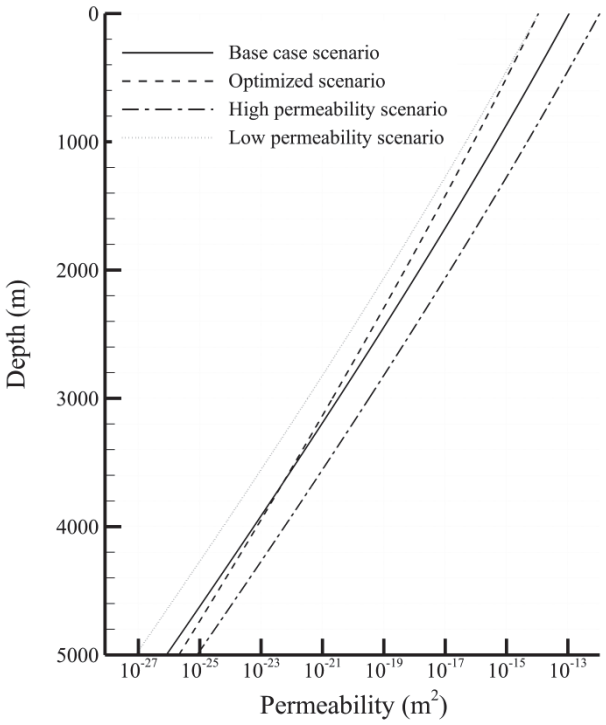

Figure 9. Initial permeability profiles used in the base case, optimized, high permeability and low permeability scenarios.

In the base case scenario, k_0 was set equal to 1.1×10^{-13} m^2, the average permeability of the upper Red fault during a fluid expulsion event as estimated by Losh et al. (1999), which is somewhat lower than the value of $k_0 = 6.68\times10^{-13}$ m^2 estimated by Revil and Cathles (2002). The base case scenario also utilized the σ^* value of 0.25 MPa estimated by Revil and Cathles (2002) for the Red fault. Porosity in all four scenarios was initially set to vary exponentially from 40% at the seafloor to 25% at a depth of 5 km

according to a best curve fitting of data reported by Hart et al. (1995). For all four scenarios, the initial Darcy velocity of oil in the lower part of the profile is very low, ranging from only 4×10^{-4} to 4×10^{-6} m/Myr at a depth of 4.5 km where hydrocarbons are thought to be sourced in the Eugene Island minibasin. This means that in the absence of any other more efficient flow mechanisms, hydrocarbons would not yet have had time to ascend the kilometer scale distances needed to reach Plio-Pleistocene reservoirs within the 3.6 million year lifespan of the Eugene Island minibasin.

A constant pressure generation rate over time was centered at a depth of 4.5 km, decreasing in Gaussian fashion to effectively zero in both the upward and downward directions over a distance of about 200 m from the maximum value. The maximum pressure generation rate for the base, high and low permeability scenarios was 9.59×10^{-7} and 1.92×10^{-6} Pa/s for the optimized scenario, based on the results of the two-dimensional basin evolution modeling described above. Temperature was set to vary with depth at a gradient of 33° C/km (Nunn et al., 1984) and was held constant over time.

The accuracy of the numerical solution to equations (1)-(9) was found to be very sensitive to nodal spacing and time step size, as illustrated in plots of these parameters versus wave velocity in figure 10. All of the simulation results reported here are based on nodal spacing values of 0.1 m and time step sizes of 0.01 yr at which the accuracy of the numerical solution stabilized.

4.3. Results

Figure 11 shows simulated changes in pore fluid pressure over a depth interval of 2 to 5 km and a time period of one million years for the base case simulation. By 100,000

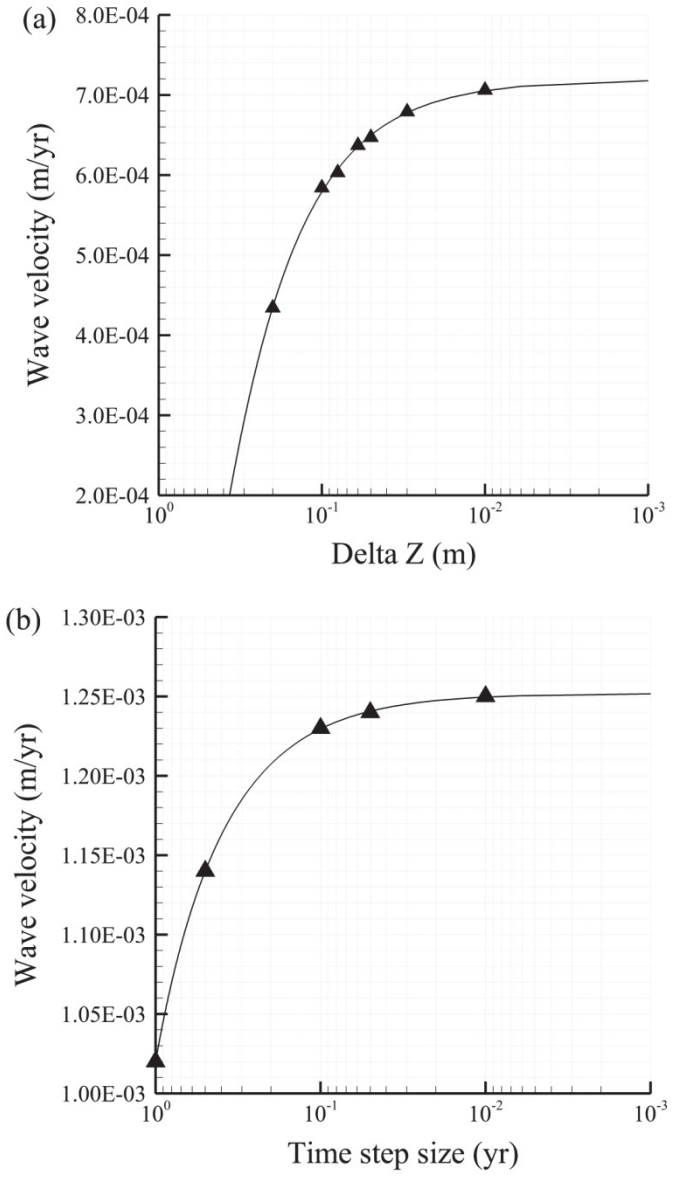

Figure 10. Solitary wave velocity as (a) a function of nodal spacing at a constant time step size of 0.01 yr, and (b) a function of time step size at a constant nodal spacing of 0.1 m.

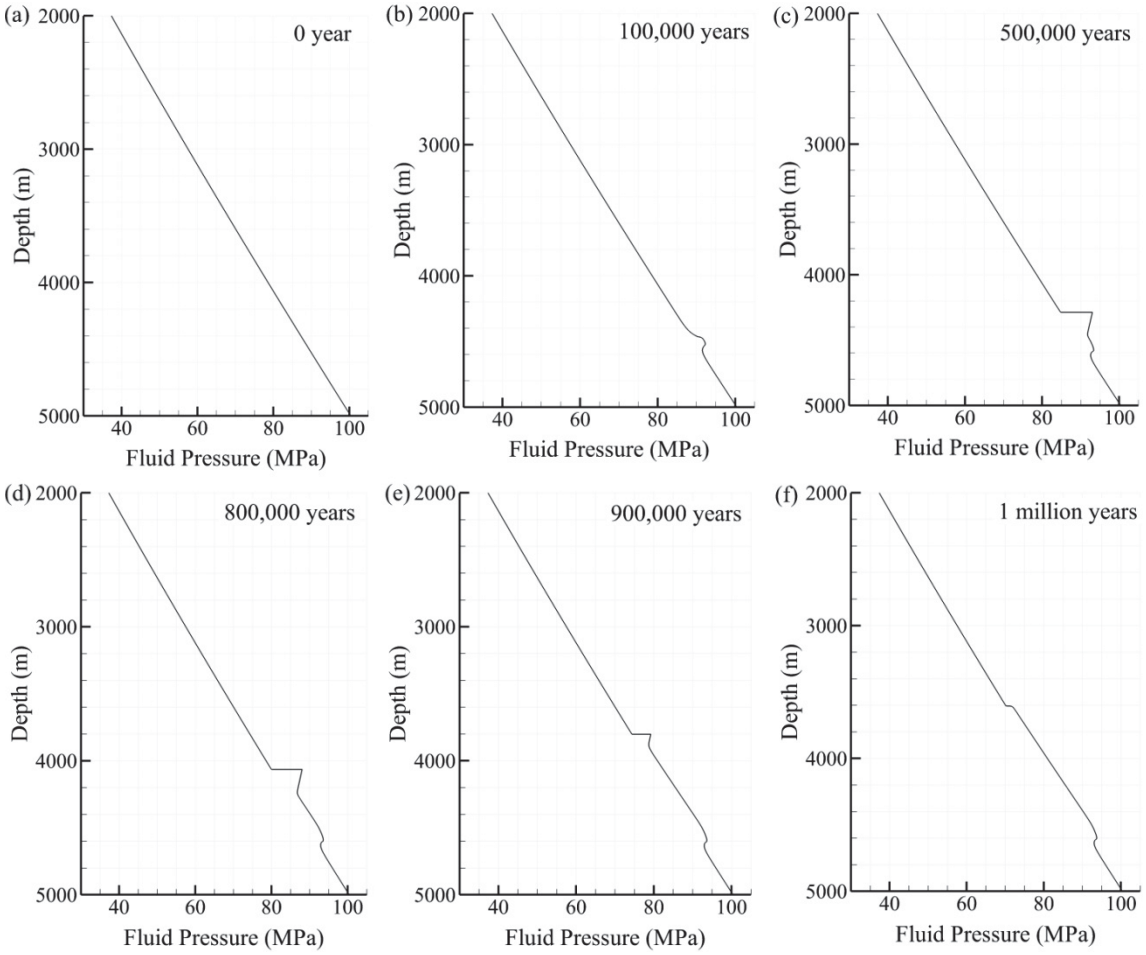

Figure 11. Plots of fluid pressure as a function of depth showing the propagation of a solitary wave at (a) time = 0, (b) 100,000 years, (c) 500,000 years, (d) 800,000 years, (e) 900,000 years, and (f) 1 million years for the base case scenario.

years, a significant perturbation of 1-2 MPa in the initially linear pressure-depth profile is visible at 4.5 km, corresponding to the location at which the pressure generation source is centered. Pressure continues to increase at this location over time, and by 500,000 years the zone of elevated pressure has begun to migrate upward as a solitary wave. Sensitivity analysis showed a key requirement for solitary wave formation to be a sufficiently low

background permeability of the porous medium to prevent pressure in the solitary wave from dissipating into the surroundings faster than it is being generated. Noticeable movement of the solitary wave does not occur until fluid pressure in the wave has increased enough (to about 7 MPa) and therefore effective stress has decreased enough to raise permeability significantly above the background value (see equation 2). As predicted by Rice (1992), the results of the present study confirmed the necessity for permeability to be a sensitive function of effective stress in order for solitary waves to form. When a linear relationship between permeability and effective stress was employed, solitary waves did not form for any model conditions tried.

As the solitary wave ascends into regions of lower fluid pressure and higher background permeability, the wave's amplitude decreases and it leaves behind a wake of slightly elevated fluid pressure relative to the initial fluid pressure profile. The solitary wave is able to travel to a depth of about 3.6 km in about 1 million years before the wave loses its discrete form. Although fluid pressure was continually generated in the source region centered at a depth of 4.5 km, no further solitary waves were formed over time spans on the order of millions of years. As noted above, solitary wave formation is very sensitive to the initial background fluid pressure and permeability. Fluid pressure and therefore permeability in the wake in this case remain high enough to allow further pressure increases to dissipate before consolidating into a discrete wave form.

Solitary waves are manifest as regions of elevated porosity as well as elevated fluid pressure, as follows from equation (4) and as illustrated in figure 12. Porosity initially decreases nearly linearly with depth to a minimum of about 24% at 5 km.

Porosity increases to a maximum of about 5% above the initial background value near the pressure generation source at 4.5 km. The porosity increase above the initial background subsequently diminishes with time as the solitary wave ascends, leaving a wake of porosity increase of about 1-2%.

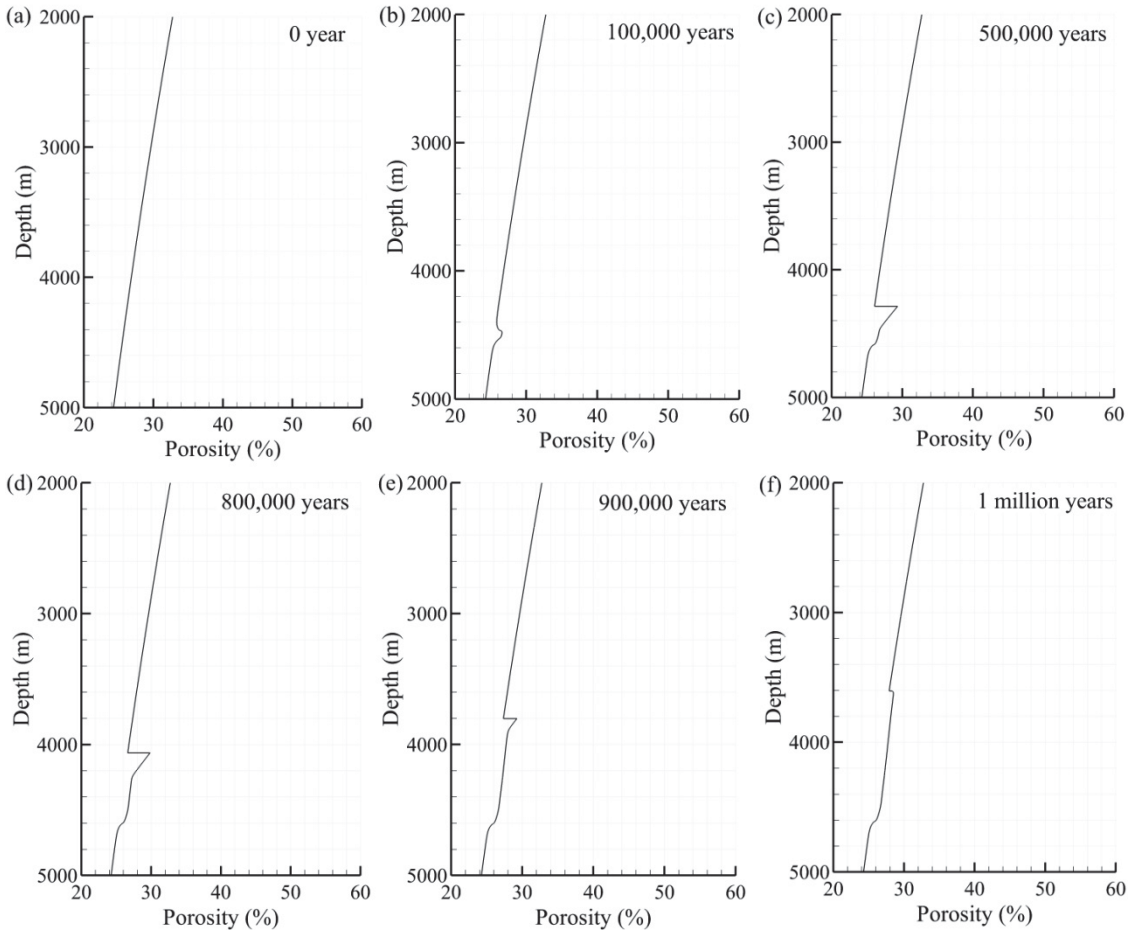

Figure 12. Plots of porosity as a function of depth showing the propagation of a porosity wave at (a) time = 0, (b) 100,000 years, (c) 500,000 years, (d) 800,000 years, (e) 900,000 years, and (f) 1 million years for the base case scenario.

The porosity profile can be used to assess the fluid transport capacity of the solitary wave. Before dissipating completely into the surrounding medium, the wave travels a vertical distance of about 1 km from its source region at a velocity increasing from about 4×10^{-4} to 2.6×10^{-3} m/yr over 500,000 years (Figure 13) due to increasing permeability with decreasing depth. Although wave amplitude decreases as the wave ascends, the wave's volumetric flow (calculated assuming a spherical three dimensional wave geometry) increases with decreasing depth because of the rapidly increasing wave velocity, until the wave dissipates to background fluid pressure and porosity levels.

In order to optimize solitary wave formation and transport, an "optimized" scenario was simulated in which the pressure generation rate, sediment bulk compressibility, and surface temperature were doubled, the background pressure was increased slightly from 93% to 95 % of lithostatic, and the compaction factor (σ^*) was decreased from 0.25 MPa to 0.2 MPa relative to the base case scenario values. Compared to the base case scenario, solitary wave formation and migration are more rapid and the distance traveled by the wave is greater in the optimized scenario, though the wave dissipates slightly sooner—after about 900,000 years instead of 1 million years (Figures 11, 14). However, after 900,000 years in the optimized scenario, the wave has ascended to a depth of about 2500 m, about twice as far as it ascended in the base case scenario. Correspondingly, the average velocity of the wave in the optimized scenario is about 0.0019 m/yr, which is approximately twice the average velocity of the wave in the base case scenario. In addition, the average volumetric flow rate of 940 m^3/yr in the optimized scenario is approximately three times greater than the average volumetric flow rate

calculated for the base case scenario.

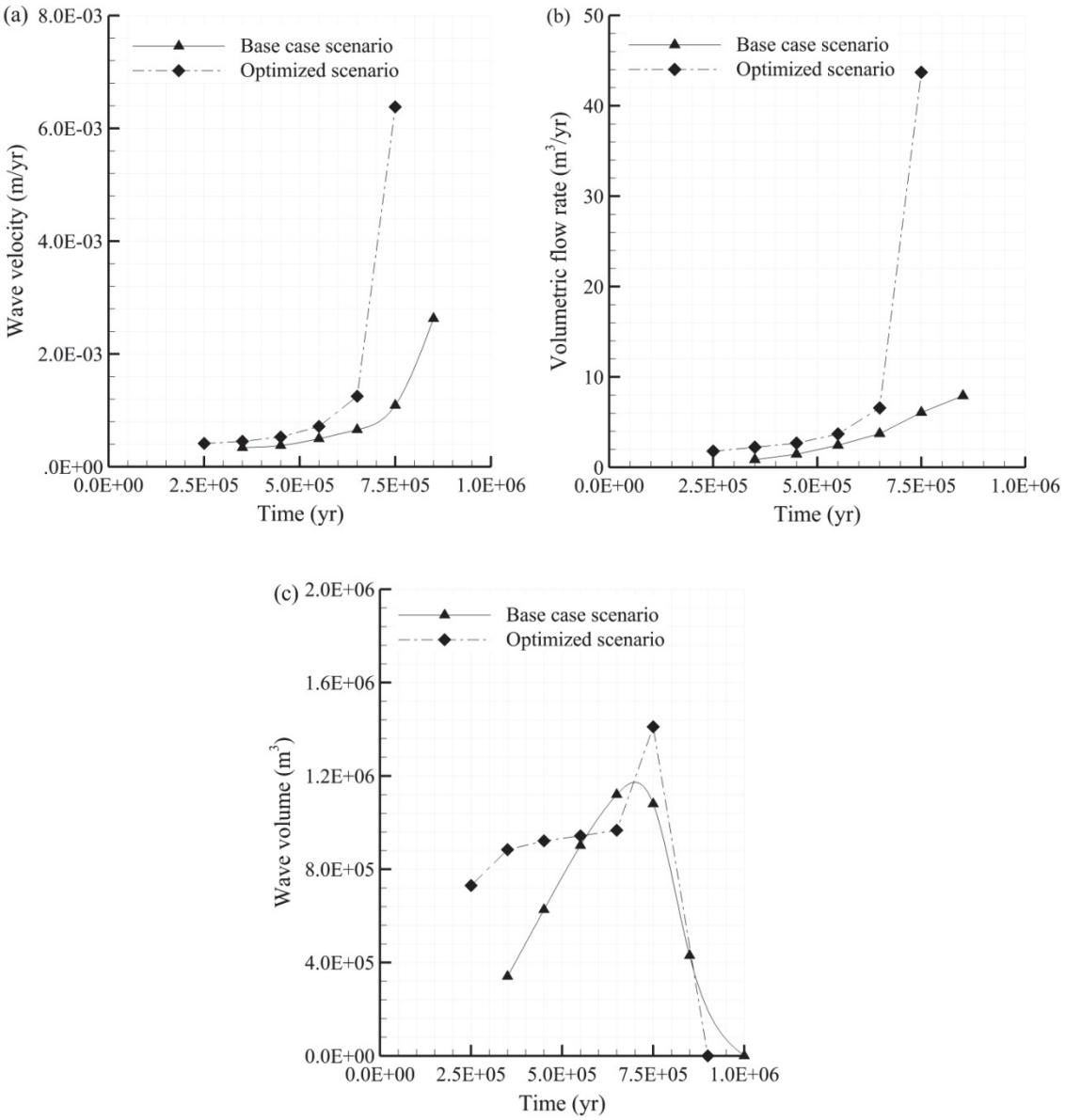

Figure 13. Plots showing (a) wave velocity, (b) wave volumetric flow rate, and (c) wave volume as a function of time for the base case and optimized scenarios.

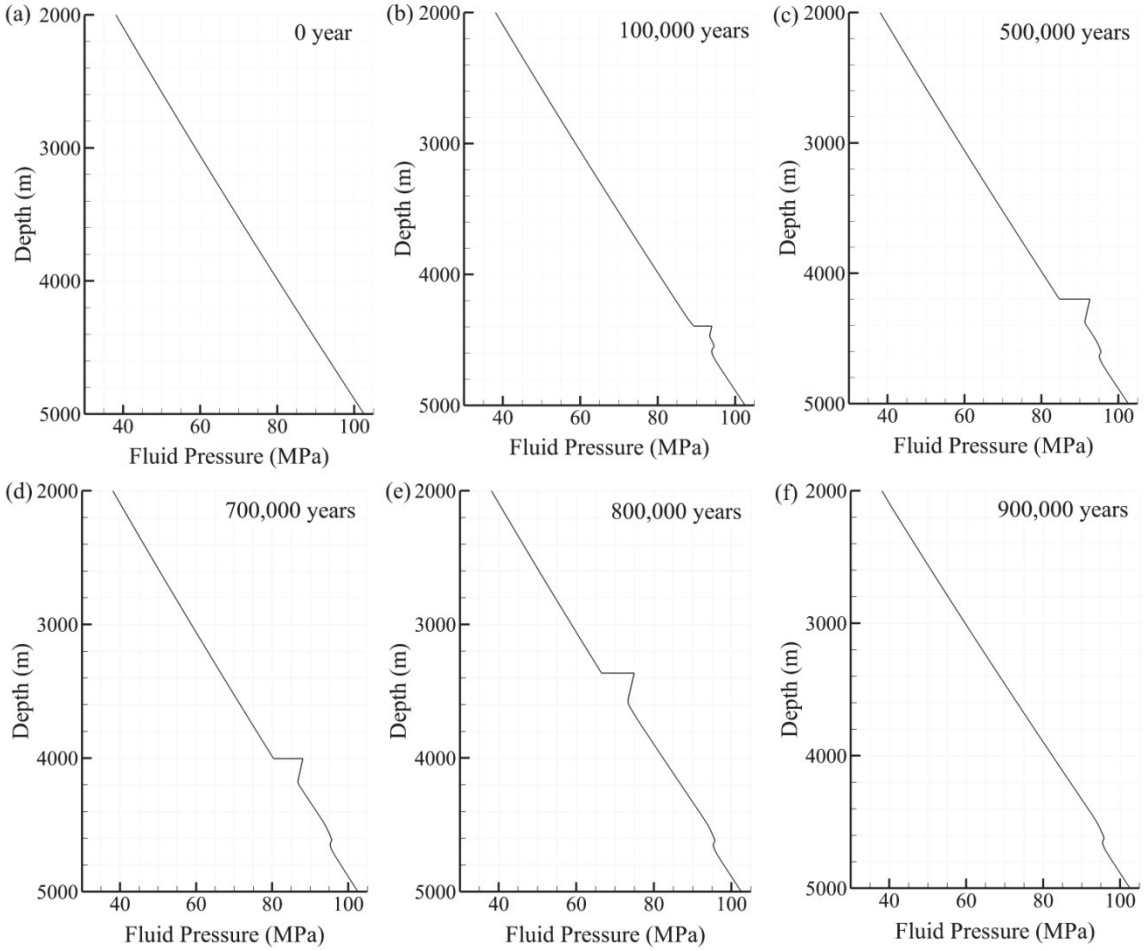

Figure 14. Plots of fluid pressure as a function of depth showing the propagation of a solitary wave at (a) time = 0 , (b) 100,000 years, (c) 500,000 years, (d) 700,000 years, (e) 800,000 years, and (f) 900,000 years for the optimized scenario.

A "high permeability" scenario was simulated in which k_0 was increased from 1.1×10^{-13} to 1.1×10^{-12} m^2 and the remaining model parameters were left the same as in the base case scenario (Table 2). This order of magnitude increase in permeability with depth relative to the base case scenario (Fig. 9) prevented any solitary waves from

forming over the one million year duration of the simulation (Fig. 15). Fluid pressure clearly increases in the source region at a depth of about 4.5 km at early times. However, the higher fluid pressure diffuses into the surroundings, forming a broad plateau of elevated fluid pressure without ever coalescing into a discrete wave form. The permeability in the source region in this scenario is only about 10^{-24} m^2, which indicates that inelastic porous media solitary waves are only able to form at very low permeabilities.

A "low permeability" scenario was simulated in which k_0 was decreased to 1.1×10^{-14} m^2, keeping the remaining parameters the same as in the base case scenario (Table 2). This resulted in an order of magnitude decrease in permeability with depth across the model profile relative to the base case scenario (Fig. 9). Figure 16 shows that a discrete solitary wave develops in the pressure generation source region, growing to large amplitude without diffusing into the surroundings. However, the wave migrates less than 100 meters within two million years of simulation time. The lower permeability inhibited fluid pressure diffusion, allowing the wave to reach larger amplitude than in the base case scenario. However, the lower permeability also slowed the migration of the wave enough such that it would not be able to travel the kilometer-scale distances needed to reach the Plio-Pleistocene reservoirs within the lifetime of the Eugene Island minibasin.

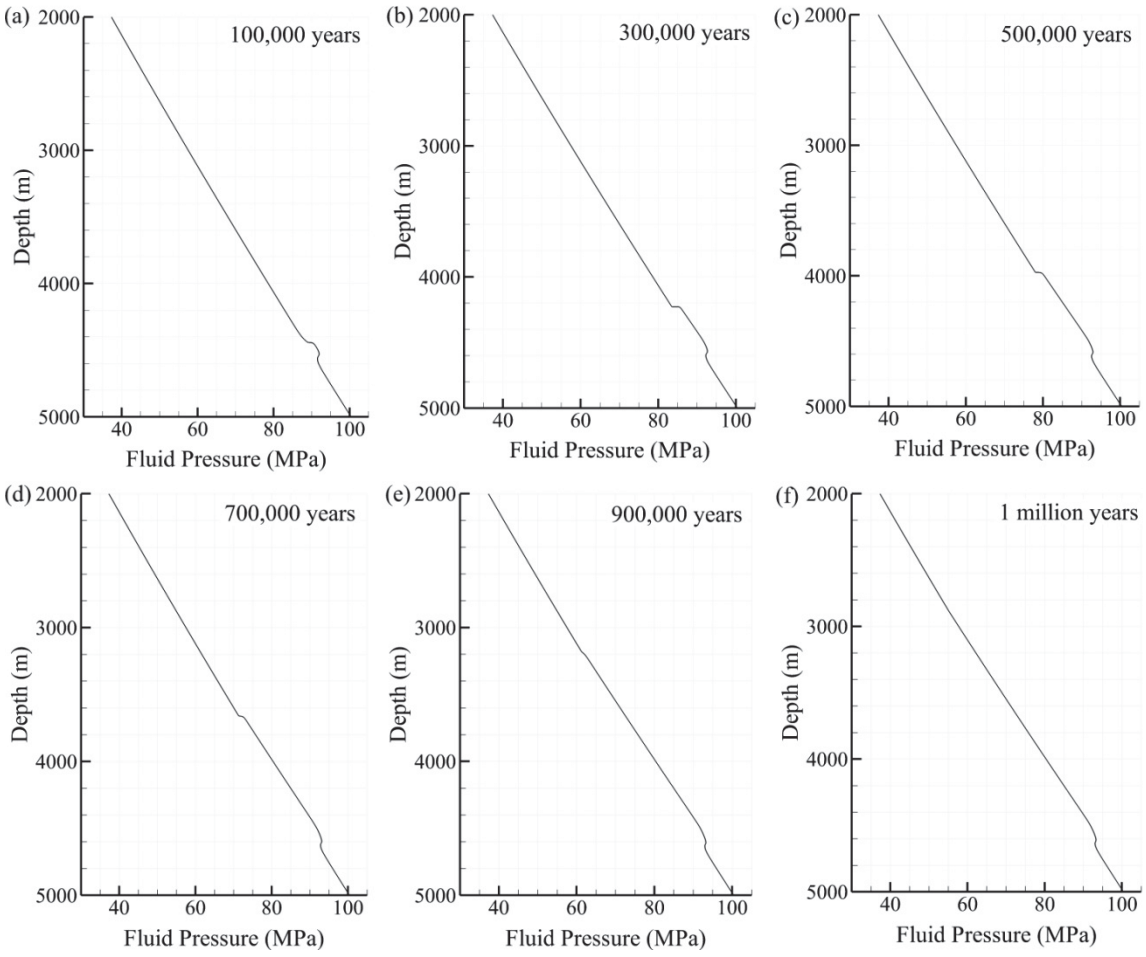

Figure 15. Plots of fluid pressure as a function of depth showing diffusion of high pressure zone without solitary wave formation after (a) 100,000 years, (b) 300,000 years, (c) 500,000 years, (d) 700,000 years, (e) 900,000 years, and (f) 1 million years for the high permeability scenario.

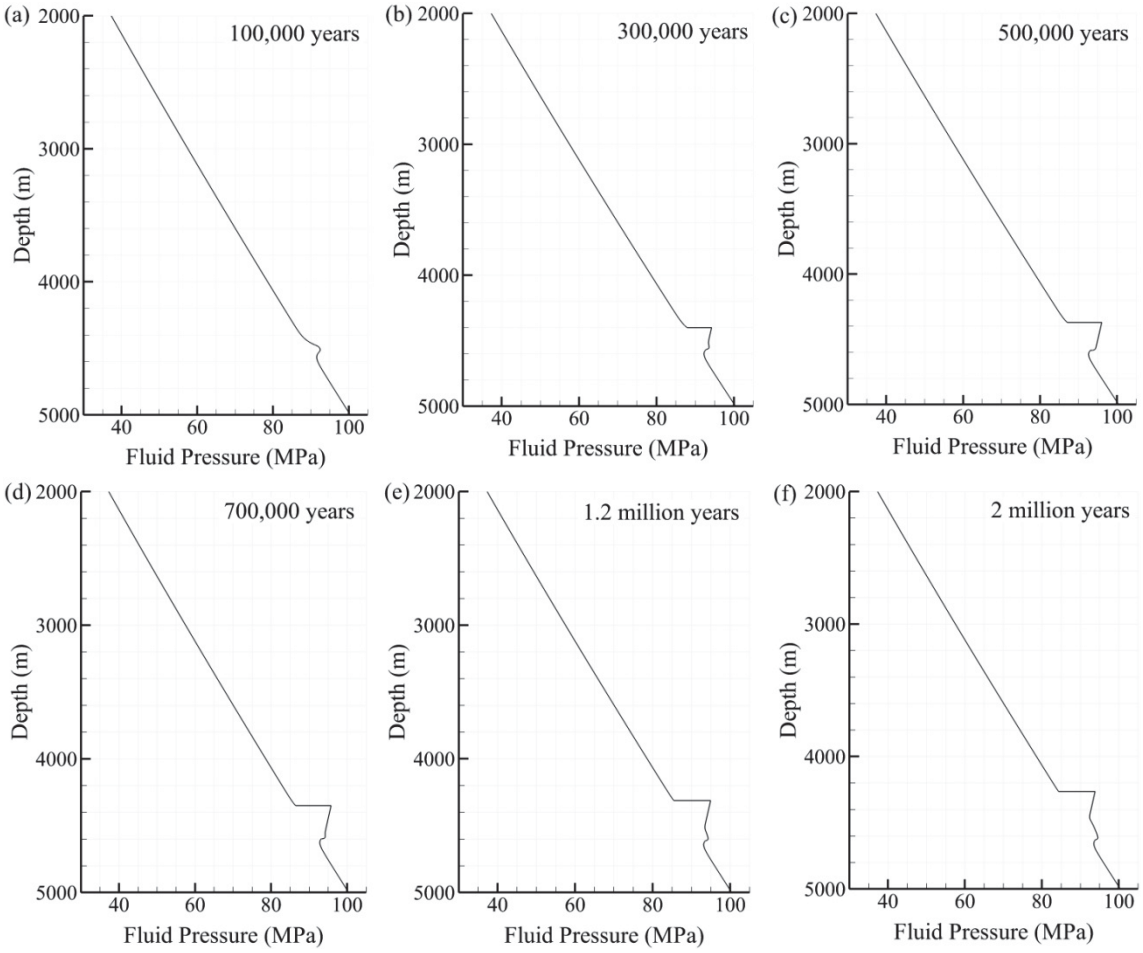

Figure 16. Plots of fluid pressure as a function of depth showing solitary wave formation after (a) 100,000 years, (b) 300,000 years, (c) 500,000 years, (d) 700,000 years, (e) 1.2 million years, and (f) 2 million years for the low permeability scenario.

5. Discussion

The results presented above indicate that petroleum-saturated solitary waves could form and migrate under conditions that could have existed during at least part of the history of the Eugene Island minibasin. This range of conditions however is narrow and likely to have existed only in the lower 1-2 kilometers of the minibasin during the latter stages of its history. The principal factor controlling solitary wave formation and migration is permeability. Foremost, as noted by Rice (1992), permeability must be a sensitive function of fluid pressure or effective stress for solitary waves to form. Sensitivity analysis in the present study showed that when permeability was independent of or varied linearly with effective stress, solitary waves did not form. For the exponential permeability-effective stress relationship utilized in the present models, at permeability greater than about 10^{-24} m^2, high fluid pressures generated in the pressure source region in the models diffused into the surroundings without coalescing into a discrete, moving wave form. At permeability lower than about 10^{-25} m^2, a high amplitude wave was able to grow in the pressure source region but it was only able to move at a rate of 10's of meters per million years, too slow to travel the kilometer-scale distances needed to reach the shallow Plio-Pleistocene reservoirs within the lifespan of the minibasin. The sensitivity of solitary waves to permeability means that they were not able to ascend more than 1-2 kilometers before permeability had increased to levels too high for the waves to continue to exist (Fig. 9). Thus, based on the results of this study, solitary waves are unlikely to have been able to deliver oil to any but perhaps the lowest of the Plio-Pleistocene reservoirs at Eugene Island if the sediments behaved elastically.

Other factors were found to affect solitary wave behavior insofar as they affect permeability through equation (2). The compaction factor, σ^*, could not vary from 0.25 MPa by more than a few ten's of kPa for solitary waves to form and migrate, otherwise permeability in the pressure source region in the models would fall outside of the ideal 10^{-25} to 10^{-24} m^2 range. Similarly, high background fluid pressures between about 91-93% of lithostatic were needed; otherwise the effective stress would take on a value that would cause the permeability to lie outside the ideal range.

Solitary wave behavior was also found to be sensitive to the value of the bulk compressibility, β_b. In all of the models presented above, a relatively high bulk compressibility of 10^{-8} Pa^{-1} was used, consistent with semi-consolidated clay (Domenico and Mifflin, 1965). Increasing the bulk compressibility by an order of magnitude caused a corresponding increase in the specific storage, S_s, and decrease in the hydraulic diffusivity,

$$D = \frac{K}{S_s} \tag{10}$$

where $K = k\rho_f g/\mu$ is the hydraulic conductivity. Sensitivity analysis showed that this lower hydraulic diffusivity allowed the solitary wave to grow to large amplitude by inhibiting the diffusion of high fluid pressure from the pressure source region. However, as for the "low permeability" scenario discussed above, the solitary wave did not move a significant distance over time scales of millions of years. Conversely, decreasing the bulk compressibility by an order of magnitude caused the hydraulic diffusivity to increase correspondingly, which caused high fluid pressure generated in the source region to diffuse into the surroundings without forming a coherent, mobile solitary wave.

In contrast to viscous porous media in which trains of waves with successively smaller amplitudes are formed (Appold and Nunn, 2002), for the elastic porous media in the present models only a single wave was formed over million year time scales from each pressure-porosity perturbation. This reduces the oil transport potential of solitary waves in elastic porous media relative to viscous porous media. Nonetheless, solitary waves in elastic porous media can be significant agents of oil transport, though probably not to the degree needed to account for the volume of oil in the Eugene Island reservoirs. The predicted solitary wave velocities of order 10^{-4} to 10^{-3} m/yr (Fig 13a) are 8 to 9 orders of magnitude greater than would be expected in the background flow regime. Volumetric flow rates of order 10^{0} m^3/yr for lengths of time on the order of 10^{5} years could thus transport volumes of oil of order 10^{5} m^3. For the approximately 100 million m^3 (645 million bbls) of oil estimated originally to have been contained in the Eugene Island reservoirs (Holland et al., 1990), hundreds of solitary waves of this size would have been needed to deliver the estimated amount of oil from the source region. Based on the present modeling results, it is unlikely that solitary waves could have been generated with this frequency at Eugene Island.

Solitary wave velocities much greater than those found in the present study have been reported from analytical solutions to differential pore fluid mass balance equations similar to equation (1). Using the following equation,

$$v = \left(\frac{\rho_f g}{\mu}\right)\left(\frac{F\left(\sigma_{e_f}\right) - F\left(\sigma_{e_0}\right)}{G\left(\sigma_{e_f}\right) - G\left(\sigma_{e_0}\right)}\right) \qquad (11)$$

Rice (1992) predicted solitary wave velocities (v) of order 10^1 to 10^3 m/yr to be possible in the San Andreas Fault zone. In equation (11), σ_{e_0} and σ_{e_f} represent effective stress immediately in front of the wave and behind the wave, respectively, F represents permeability as a function of effective stress as shown in equation (2), and G represents a porosity-effective stress relationship. Revil and Cathles (2002) defined G as

$$G = \phi = \phi_0(1 - \beta_b \sigma_e) \qquad (12)$$

and predicted solitary wave velocities of order 10^3 to 10^5 m/yr to be possible in the Red fault at Eugene Island using an equation of the form,

$$v = \left(\frac{1-\phi_0}{\phi_0}\right)\frac{gk_0(\rho_g - \rho_f)}{\mu\beta_b\sigma_0} \qquad (13)$$

where σ_0 is an "effective stress shock" that is not explicitly defined.

The reason for the low wave velocities predicted in the current study can be understood by considering equation (11). When effective stress is high, which is expected at great depths even for relatively high degrees of overpressuring, then the permeability (F) is driven to low values. Because of the high sensitivity of permeability with respect to effective stress in equation (2), solitary wave velocity would tend to increase rapidly with decreasing depth. However as discussed above, as permeability increases, hydraulic diffusivity increases such that fluid pressure diffuses into the background before a solitary wave can coalesce and migrate, unless the pressure generation rate increases correspondingly. Based on the present modeling, it seems unlikely that pressure generation would have exceeded rates of order 10^{-6} Pa/s in the hydrocarbon source region at Eugene Island, such that solitary waves are unlikely to have been able to reach velocities higher than the order 10^{-3} m/yr velocities modeled. These

model velocities are also in good agreem ent with those obtained from Rice's (1992) analytical solution when the effective stress values corresponding to the boundaries of the wave in the model (Fig. 17) are employed in equation (11).

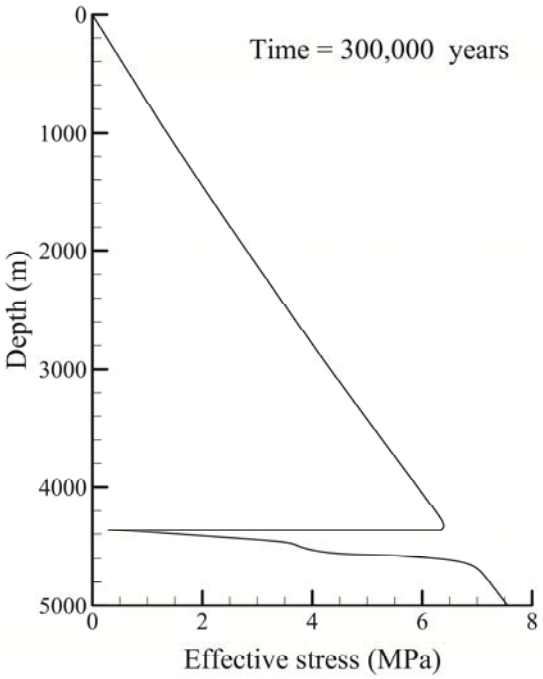

Figure 17. Plot of ef fective stress as a function of depth at time = 300,000 years for a base case scenario in which significant perturbation in the effective stress profile occurred at oil source depth of 4.5 km due to solitary wave formation.

Although solitary waves are unlikely to have been im portant mechanisms of oil transport between the hypothesized source region at 4.5 km depth and the principal reservoirs at Eugene Island for sedim ents with elastic rheology, it is possible that they could be important in other locations where the distance between the hydrocarbon source

region and reservoir is smaller. However, the narrow range of low permeabilities needed for their formation and migration indicates that they are likely to be relatively rare phenomenon. Solitary waves may be better transport agents for methane, whose lower density and viscosity might lead to significantly greater wave velocities and is a subject that should be investigated in future research.

6. Conclusions

Two-dimensional numerical modeling of sedimentation, compaction, hydrocarbon generation, fluid flow, and heat transport in the Eugene Island minibasin indicate that Early Tertiary hydrocarbon source sediments would have experienced pore fluid pressure increases averaging about 10^{-6} Pa/s, building to excess fluid pressures of about 52 MPa by the present day. Most of this excess fluid pressure was predicted to be caused by compaction disequilibrium with the remainder caused by hydrocarbon formation. Based on extrapolations from empirical data in the upper 2.5 km of the present day minibasin using equation (2), permeability in the hydrocarbon source region around 4.5 to 4.8 km depth was predicted to be very low, between about 10^{-25} and 10^{-24} m^2. At such low permeabilities, fluids in the hydrocarbon source region would have been essentially immobile over the 3.6 million year lifespan of the minibasin, with predicted flow velocities only on the order of 10^{-6} m/Myr or less. Oil saturated solitary waves, however, could travel much faster through such low permeability material, with predicted velocities on the order of 10^{-3} m/yr, about nine orders of magnitude greater. Solitary waves could only form when the pressure generation rate in the hydrocarbon source region was high compared to the pressure diffusion rate as governed by the hydraulic diffusivity, which in turn was governed primarily by variations in permeability. When permeability in the source region was greater than about 10^{-24} m^2, then high fluid pressures generated there diffused into the background before coalescing into a mobile solitary wave. When permeability was lower than about 10^{-25} m^2, a high amplitude solitary wave formed but it did not move more than a few tens of meters over million

year time scales. The necessary permeability range was reached in the source region only at high degrees of overpressuring between about 91 and 93% of lithostatic. As a solitary wave ascended to shallower depths where permeability was higher, the wave's amplitude decreased in size until it finally completely dissipated into the background within 1-2 km of travel distance, leaving a wake of slightly elevated fluid pressure. This wake of elevated fluid pressure prevented further solitary wave formation over the lifespan of the minibasin, making solitary wave formation a one-time event. The infrequency of solitary wave formation, coupled with the short distances that they are able to travel and relatively small volumes indicates that oil saturated solitary waves are unlikely to have played an important role in charging the shallow Pleistocene reservoirs at Eugene Island. Solitary waves could perhaps be efficient more important mechanism for oil transport in other locations where reservoirs and source rocks are separated by less than a kilometer.

References

Alexander, L., Flemings, P. B. (1995) Geologic evolution of a Pliocene–Pleistocene salt-withdrawal minibasin, Eugene Island South Addition, Block 330, offshore Louisiana. American Association of Petroleum Geologists Bulletin, 79, pp. 1737–1756.

Alexander, L., Handschy, J. (1998) Fluid flow in a faulted reservoir system, South Eugene Island Block 330 field, offshore Louisiana. American Association of Petroleum Geologists Bulletin, 82, No.3, pp. 387–411.

Anderson, R.N., He, W., Hobart, M.A., Wilkinson, C.R., Nelson, H.R. Jr. (1991) Active fluid flow in the Eugene Island Area, offshore Louisiana. Geophysics: The Leading Edge, 10, No. 4, pp. 12–17.

Anderson, R. N., Flemings, P., Losh, S., Austin, J., Woodhams, R. (1994) Gulf of Mexico growth fault drilled, seen as oil, gas migration pathway. Oil and Gas Journal, 92, No. 23, pp. 97–104.

Appold, M. S., Nunn, J. A. (2002) Numerical models of petroleum migration via buoyancy-driven porosity waves in viscously deformable sediments. Geofluids, 2, pp. 233–247.

BasinMod1-D® (2009) BasinMod 1-D petroleum systems software documentation: Platte River Associates, unpublished user guide, pp. 576.

BasinMod2-D® (2009) BasinMod 2-D petroleum systems software documentation: Platte River Associates, unpublished user guide, pp. 604.

Bourlange, S., Henry, P. (2007) Numerical model of fluid pressure solitary wave propagation along the décollement of an accretionary wedge: application to the Nankai wedge. Geofluids, 7, pp. 323–334.

Bethke, C. M. (1985) A numerical model of compaction-driven groundwater flow and heat transfer and its application to the paleohydrology of intracratonic sedimentary basins. Journal of Geophysical Research, 90, pp. 6817–6828.

Curtis, D.M. (1991) The northern Gulf of Mexico basin. In: Economic Geology, US. The Geology of North America, P-2 (eds Gluskoter HJ, Rice DD, Taylor RB), pp. 301–324. Geological Society of America, Boulder, Colorado.

Domenico, P.A., Mifflin, M.D. (1965) Water from low permeability sediments and land subsidence. Water Resources Research, 4, pp. 563-576.

Dow, W. G. (1984) Oil source beds and oil prospect definition in the upper Tertiary of the

Gulf coast. Gulf Coast Association of Geological Societies Transactions, 34, pp. 329–339.

Fetter, C.W. (2001) Applied Hydrogeology (4th edition). Prentice-Hall, Upper Saddle River, New Jersey, 598p.

Freeze, R.A., Cherry, J.A. (1979) Groundwater, New Jersey: Prentice Hall, 604 pp.

Gordon, D. S., Flemings, P. B. (1998) Generation of overpressure and compaction-driven fluid flow in a Plio-P leistocene growth-faulted basin, Eugene Island 330, of fshore Louisiana. Basin Research, 10, pp. 177–196.

Guerin, G. (2000) Acoustic and thermal characterization of oil migration, gas hydrates formation and silica diagenesis, PhD. Thesis, Columbia University.

Haney, M. M., Snieder, R., Sheiman, J., Losh, S. (2005b) A moving fluid pulse in a fault zone. Nature, 437, 46.

Hart, B. S., Flemings, P.B., Deshpande, A. (1995) Porosity and pressure: Role of compaction disequilibrium in the development of geopressures in a Gulf Coast Pleistocene basin. Geology, 23, pp. 45–48.

Holland, D. S., Nunan, W. E., Lammlein, D. R., Woodhams, R. L. (1980) Eugene Island Block 330 Field, of fshore Louisiana. In Giant Oil and Gas Fields of the Decade, 1968–1978 (ed. M. T. Halbouty), Memoir 30, pp. 253–289. American Association of Petroleum Geologists.

Holland, D. S., Leedy, J. E., Lammlein, D. R. (1990) Eugene Island Block 330 Field—USA, offshore Louisiana. In AAPG Treatise of Petroleum Geology, Atlas of Oil and Gas Fields, Structural Traps III, pp. 103–143. American Association of Petroleum Geologists.

Ingebritsen, S., Sanford, W., Neuzil, C. (2006) Groundwater in geologic processes, 2nd edn. Cambridge University Press, Cambridge, 536 pp.

Lin, G., Nunn, J. A. (1997) Evidence for recent migration of geopressured fluids along faults in Eugene Island, Block 330, of fshore Louisiana from estimates of pore water salinity. Gulf Coast Association of Geological Societies Transactions, 47, pp. 419–424.

Losh, S., Eglinton, L., Schoell, M., Wood, J. (1999) Vertical and lateral fluid flow related to a large growth fault, South Eugene Island Block 330 field, of fshore Louisiana. American Association of Petroleum Geologists Bulletin, 83, pp. 244–276.

Matthai, S.K., Roberts, S.G. (1996) The influence of fault permeability on single-phase

fluid flow near fault-sand interactions: Results from steady-state high-resolution models of pressure-driven fluid flow. American Association of Petroleum Geologists Bulletin, 80, No. 11, pp. 1763–1779.

Middleton, G.V., Wilcock, P.R. (1994) Mechanics in the Earth and Environmental Sciences. Cambridge University Press, Cambridge.

Nunn J.A., Scardina, A.D., Pilger, R.H., Jr. (1984) Thermal evolution of the north-central Gulf Coast. Tectonics, 3, pp. 723–40.

Revil A., Cathles, L.M. III (2002) Fluid transport by solitary waves along growing faults; a field example from the South Eugene Island Basin, Gulf of Mexico. Earth and Planetary Science Letters, 202, pp. 321–335.

Rice, J. (1992) Fault stress states, pore pressure distributions, and the weakness of the San Andreas Fault. In: Fault Mechanics and Transport Properties of Rocks (eds Evans B, Wong TF), pp. 475–503. Academic Press, London.

Roberts, S. J., Nunn, J. A. (1995) Episodic fluid expulsion from geopressured sediments. Marine and Petroleum Geology, 12, pp. 195–204.

Roberts, S. J. (2001) Fluid flow in the South Eugene Island area, offshore Louisiana: results of numerical simulations. Marine and Petroleum Geology, 18, pp. 799–805.

Robie, R. A., Hemingway, B. S., Fisher, J. R. (1979) Thermodynamic properties of minerals and related substances at 298.15 K and 1 bar (10^5 Pascal) pressure and at higher temperatures. U.S. Geological Survey Bulletin 1452.

Sclater, J. G., Christie, P.A.F. (1980) Continental stretching: an explanation of the post-mid-Cretaceous subsidence of the central North Sea basin. Journal of Geophysical Research, 85, No. B7, pp. 3711–3739.

Schwartz, F.W., Zhang, H. (2003) Fundamentals of Groundwater: John Wiley & Sons, New York, 583 pp.

Stump, B. B., Flemings, P. B. (2002) Consolidation state, permeability, and stress ratio as determined from uniaxial strain experiments on mudstone samples from the Eugene Island 330 area, Offshore Louisiana, in A. R. Huffman and G. L. Bowers, eds., Pressure regimes in sedimentary basins and their prediction: AAPG Memoir 76, pp. 131–144.

Sweeney, J. J., Burnham, A.K. (1990) Evaluation of a simple model of vitrinite reflectance based on chemical kinetics. American Association of Petroleum Geologists Bulletin, 74, No. 10, pp. 1559–1570.

Thompson, K.F.M. (1988) Gas-condensate m igration and oil fractionation in deltaic systems. Marine and Petroleum Geology, 5, pp. 237–246.

Thompson, K.F.M. (1991) Petroleum classification based on the ratio of sulfur to nitrogen; application in the East Texas basin. Transactions – Gulf Coast Association of Geological Societies, 41, pp. 602.

Ungerer, P., Burrus, J., Doligez, B., Chénet , P.Y., Bessis, F. (1990) Basin evolution by integrated two-dimensional modeling of heat transfer , fluid flow, hydrocarbon generation and m igration. American Association of Petroleu m Geologists Bulletin, 74, No. 3, pp. 309–335.

Whelan, J. K., Kennicutt, M. C. II, Brooks, J. M., Schum acher, D., Eglinton, L. B. (1994) Organic geochemical indicators of dynamic fluid flow processes in petroleum basins. Organic Geochemistry, 22, pp. 587–615.

Whelan, J. K., Eglinton, L., Kennicutt II, M. C., Qian, Y. (2001) Short-time-scale (year) variations of petroleum fluids from the U.S. Gulf Coast. G eochimica et Cosmochimica Acta, 65, No. 20, pp. 3529–3555.

Young, A., Monaghan, H., Schweisber ger, R.T. (1977) Calculation of ages of hydrocarbons in oils; physical chem istry applied to petroleum geochemistry. American Association of Petroleum Geologists Bulletin, 61, pp. 573–600.

APPENDIX A. Tables showing parameter values used in models

Table 1. Thermal and lithological parameters used in the BasinMod® 2-D software for base case scenario simulations.

Model lithology	Sandstone	Upper shale	Lower shale	Evaporite
Initial porosity (fraction)	0.3	0.25	0.25	0
Porosity reduction factor	1.75×10^{-4}	3.0×10^{-4}	3.0×10^{-4}	0.05
Matrix density (g/cm^3)	2.64	2.6	2.6	2.15
Kozeny-Carman grain size (mm)	0.09037	4.02×10^{-4}	1.33×10^{-7}	4.0×10^{-4}
Initial vertical permeability (m^2)	10^{-13}	10^{-18}	1.1×10^{-25}	1.0×10^{-21}
Vertical: horizontal permeability	0.4	0.2	0.2	1
Permeability reduction factor	7	6	6	1
Matrix thermal conductivity ($W\ m^{-1}\ K^{-1}$)	3.34	1.82	1.82	5.4
Vertical: horizontal matrix thermal conductivity	1.55	1.55	1.55	1.55
Matrix heat capacity ($kJ\ m^{-3}\ K^{-1}$)	2800	2100	2100	1750
Fracture gradient factor	0.2	0.8	0.8	0.9
Irreducible water saturation	0.1	0.8	0.8	1
% TOC	0	0.55	0.55	0

Table 2. Parameter values used in the solitary wave calculations.

Parameters	**Base case scenario**	**Optimized scenario**	**High permeability scenario**	**Low permeability scenario**
Pressure generation rate (Pa/s)	9.59×10^{-7}	1.92×10^{-6}	9.59×10^{-7}	9.59×10^{-7}
Surface permeability, k_0 (m^2)	1.1×10^{-13}	1.1×10^{-14}	1.1×10^{-12}	1.1×10^{-14}
Bulk compressibility, β_b (Pa^{-1})	1.0×10^{-8}	2.0×10^{-8}	1.0×10^{-8}	1.0×10^{-8}
Compaction factor, σ^* (MPa)	0.25	0.2	0.25	0.25
Seafloor temperature (° C)	5	10	5	5
Background pressure (% of lithostatic)	93%	95%	93%	93%
Density of oil (kg/m^3)	800			
Grain density (kg/m^3)	2650			
Oil compressibility (Pa^{-1})	5.0×10^{-10}			
Geothermal gradient (°C/km)	33			
Surface porosity (fraction)	0.4			

APPENDIX B. Fortran code for 1-D solitary wave calculations

```
C     TITLE: One-dimensional solitary wave model

C     This program calculates the fluid pressure as a function of depth
C     using the modified pore pressure diffusion equation proposed by
C     Bourlange and Henry (2007). Permeability in the model is dependent
C     on the effective stress from the relation proposed by Rice (1992).
C     The model assumes oil saturated domain with a constant fluid pressure
C     at zero and five kilometers as a Dirichlet boundary conditions.

      INTEGER NNODES, P1, PRTSTP(10), SIMPRO, TIMSTP, ITOP, IPK, IBOT,
     +  NMTOUT, TPRIVL

      PARAMETER (P1=1000000)

      DOUBLE PRECISION DELZ, DELT, PERMEA(P1), GRAVAC, VISLIQ(P1),
     +            SIMLNS, DEPTH(P1), Z(P1), ZMAX, DENLIQ,
     +            LODIAG(P1), MNDIAG(P1), UPDIAG(P1), LOAD(P1),
     +            PRSNEW(P1), FLUPRE(P1), TIME, DENBLK(P1),
     +            PERME0, SIGSTR, DARVEL(P1), EFFSTR(P1),
     +            TOTSTR(P1), PRETOP, PREBOT, SIMLNY, BKGPRE(P1),
     +            CMPBLK, CMPFLD, POROS(P1), SPECST(P1),
     +            PORBOT, PORTOP, WAVTOP, WAVBOT, WAVEPK(2),
     +            WAVLEN, WAVVOL, PI, PORSUM, WAVPOR, WVPVOL,
     +            WAVVEL, WAVTIM, WAVVFL, MAXPRE, STEMP, TEMP(P1),
     +            PREGEN(P1), DENGRN, DELPOR(P1), EFFPRE(P1),
     +            LITHFR, PREMAX

      OPEN (UNIT=12, FILE='solwave-flux-node-data', STATUS='UNKNOWN')
      OPEN (UNIT=13, FILE='solwave-flux-time-data', STATUS='UNKNOWN')

   10 FORMAT(A45, 2X, A10)
   20 FORMAT(A28, 1X, A12, 1X, A23, 1X, A24, 1X, A20, 1X, A25, 1X, A15,
     +   1X, A25,1X, A17, 1X,A24,1X,A21)
   30 FORMAT(A9, I8, 1X, A22, 1X, I4, A7)
   40 FORMAT(A22, E8.2, /)
   50 FORMAT(A24, 1X, A18, 1X, A15, 1X, A25, 1X, A23, 1X, A18, 1X, A28,
     +   1X, A24, 1X, A35)
   60 FORMAT(9(E15.7, 2X))
   70 FORMAT(A8, I5)

C     Define parameter values (SI units)

      NNODES = 50000
      PERME0 = 1.1D-13
      SIGSTR = 0.25D+06
```

```
      GRAVAC = 9.81D+00
      DENLIQ = 0.8D+03
      DENGRN = 2.65D+03
      ZMAX   = 5.0D+03
      DELZ   = ZMAX/(NNODES-1)
      CMPBLK = 1.0D-08
      CMPFLD = 5.0D-10
      STEMP  = 0.05D+02
      PI     = 3.141592654D+00
      PREMAX = 9.59D-07
      LITHFR = 0.93D+00

C     Define simulation length in years

      SIMLNY = 1.0D+06
      SIMLNS = SIMLNY*3.1536D+07
      TIMSTP = 1.0D+08
      DELT   = SIMLNS/TIMSTP

      WRITE(*,40) ' Delta t (years) = ', DELT/3.1536D+07
      WRITE(*,40) ' Nodal Spacing (m) = ', DELZ

C     Define time steps for which output is to be printed to nodal output file

      PRTSTP(1) = TIMSTP/10
      PRTSTP(2) = 2*TIMSTP/10
      PRTSTP(3) = 3*TIMSTP/10
      PRTSTP(4) = 4*TIMSTP/10
      PRTSTP(5) = 5*TIMSTP/10
      PRTSTP(6) = 6*TIMSTP/10
      PRTSTP(7) = 7*TIMSTP/10
      PRTSTP(8) = 8*TIMSTP/10
      PRTSTP(9) = 9*TIMSTP/10
      PRTSTP(10) = TIMSTP

C     Define number of time steps for which output is to be printed to time output file

      NMTOUT = 20

C     Define time step interval for which output is to be printed to time output file

      TPRIVL = TIMSTP/NMTOUT

C     Assign initial parameter values

      DO I = 1, NNODES

C           ...define elevation and depth
```

```
      Z(I) = (I-1)*DELZ
      IF (I .EQ. NNODES) THEN
        DEPTH(I) = 0.0D+00
      ELSE
        DEPTH(I) = ZMAX - Z(I)
      ENDIF

C     ...assign initial porosity (Hart et el, 2005)

      POROS(I) = 0.4D+00*(EXP(-0.1D-03*DEPTH(I)))

C     ...compute initial bulk density

      DENBLK(I) = (1 - POROS(I))*DENGRN + POROS(I)*DENLIQ

C       ...compute total stress

      TOTSTR(I) = DENBLK(I)*GRAVAC*DEPTH(I)

C     ...compute specific storage

      SPECST(I) = DENLIQ*GRAVAC*(CMPBLK + POROS(I)*CMPFLD)

C       ...assign initial pressure generation rate and fluid pressure

      PREGEN(I) = PREMAX/(DCOSH((DELZ*(I-1) - DELZ*NNODES/
     +              1.0D+01)/3.0D+01))

      FLUPRE(I) = LITHFR*DENBLK(I)*GRAVAC*DEPTH(I)

C       ...assign a reference unperturbed background fluid pressure

      BKGPRE(I) = LITHFR*DENBLK(I)*GRAVAC*DEPTH(I)

C       ...compute effective stress

      EFFSTR(I) = TOTSTR(I) - FLUPRE(I)

C       ...compute permeability (Revil & Cathles, 2002)

      PERMEA(I) = PERME0*(EXP(-EFFSTR(I)/SIGSTR))

C     ...compute subsurface temperature(Geothermal gradient = 33 Degree
C       Celsius/km)(Holland et al, 1990; Gordon & Flemings, 1998))

      TEMP(I) = STEMP + 0.33D-01*DEPTH(I)
```

```
C      ...compute fluid viscosity (Middleton & Wilcock, 1994)

         VISLIQ(I) = (1.663D+06)*((TEMP(I)+ 2.73D+02)**(-3.37D+00))

       END DO

C     Calculate initial Darcy velocity

       DO I=1, NNODES-1
         DARVEL(I+1) = -(PERMEA(I+1)/VISLIQ(I))*((FLUPRE(I+1) -
     +      FLUPRE(I))/DELZ - DENLIQ*(-1.0D+00*GRAVAC))
       END DO
       DARVEL(1) = DARVEL(2)

C     Write header for TECPLOT-formatted nodal output file

       WRITE(12,10) 'TITLE = "1D implicit fluid pressure solution:',
     +   'node data"'

       WRITE(12,20) 'VARIABLES = "Elevation (m)",', '"Depth (m)",',
     +   '"Fluid Pressure (MPa)",', '"Darcy velocity (m/yr)",',
     +   '"Permeability (m2)",', '"Effective stress (MPa)",',
     +   '"Porosity (%)",', '"Specific storage (1/m)",',
     +   '"Temperature(C)",','"Fluid Viscosity(Pa.S)",',
     +   '"Bulk Density(Kg/m3)"'

C     Write header for TECPLOT-formatted time output file

       WRITE(13,10) 'TITLE = "1D implicit fluid pressure solution:',
     +   'time data"'

       WRITE(13,50) 'VARIABLES = "Time (yr)",',
     +   '"Wave bottom (m)",',  '"Wave top (m)",',
     +   '"Wave peak position (m)",', '"Wave velocity (m/yr)",',
     +   '"Wave length (m)",', '"Average wave porosity (%)",',
     +   '"Wave pore volume (m3)",',
     +   '"Wave volumetric flow rate (m3/yr)"'

       WRITE(13,70) 'ZONE, I=', NMTOUT+1

C     Write initial conditions to TECPLOT-formatted nodal output file

       TIME = 0.0D+00

       CALL TECWRT(Z, DEPTH, FLUPRE, TIME, NNODES, DARVEL, PERMEA,
     +   EFFSTR, POROS, SPECST, TEMP, VISLIQ, DENBLK)

C     Solving for the Implicit Finite Difference Solution obtained from the
```

```
C     Pore Pressure Diffusion equation from Bourlange and Henry(2007)

C          ...Define upper and lower boundary conditions

      PREBOT = FLUPRE(1)
      PRETOP = FLUPRE(NNODES)

      PORBOT = POROS(1)
      PORTOP = POROS(NNODES)

      WAVVEL = 0.0D+00

      DO 500 N = 1, TIMSTP

       TIME = N*(DELT/3.1536D+07)

       DO I = 1, NNODES

         IF (I .EQ. 1) THEN
          LOAD(I) = PREBOT
          MNDIAG(I) = 1.0D+00
          UPDIAG(I) = 0.0D+00
         END IF

         IF (I .EQ. NNODES) THEN
          LOAD(I) = PRETOP
          MNDIAG(I) = 1.0D+00
          LODIAG(I) = 0.0D+00
         END IF

         IF ((I .GT. 1) .AND. (I .LT. NNODES)) THEN

          LODIAG(I) = PERMEA(I)/(DELZ*DELZ)

          MNDIAG(I) = -2.0D+00*PERMEA(I)/(DELZ*DELZ) -
     +        (PERMEA(I+1) - PERMEA(I))/(DELZ*DELZ) -
     +        SPECST(I)*VISLIQ(I)/(DENLIQ*GRAVAC*DELT)

          UPDIAG(I) = PERMEA(I)/(DELZ*DELZ) +
     +        (PERMEA(I+1) - PERMEA(I))/(DELZ*DELZ)

          LOAD(I) = DENLIQ*GRAVAC*((PERMEA(I+1) - PERMEA(I))/DELZ)
     +         - SPECST(I)*VISLIQ(I)*FLUPRE(I)/(DENLIQ*GRAVAC*DELT)
     +         - SPECST(I)*VISLIQ(I)*PREGEN(I)/(DENLIQ*GRAVAC)

         ENDIF

       END DO
```

```
      CALL TRIDIA(LODIAG, MNDIAG, UPDIAG, LOAD, NNODES, PRSNEW)

C     Update fluid pressure, effective stress, permeability
C     and calculate change in porosity from Hart et al (1995)

      DO I=2, NNODES-1

        FLUPRE(I) = PRSNEW(I)
        EFFPRE(I) = EFFSTR(I)

        IF (FLUPRE(I) .LT. BKGPRE(I)) THEN
          FLUPRE(I) = BKGPRE(I)
        END IF

        EFFSTR(I) = TOTSTR(I) - FLUPRE(I)

        PERMEA(I) = PERME0*(EXP(-EFFSTR(I)/SIGSTR))

        DELPOR(I) = - PORTOP*CMPBLK*(EXP(-CMPBLK*EFFSTR(I)))
     +              *(EFFSTR(I) - EFFPRE(I))

      END DO

      DO 110 I=1, NNODES

C       Update porosity

        POROS(I) = POROS(I) + DELPOR(I)

C       Update bulk density

        DENBLK(I) = (1-POROS(I))*DENGRN + POROS(I)*DENLIQ

C       Update specific storage

        SPECST(I) = DENLIQ*GRAVAC*(CMPBLK + POROS(I)*CMPFLD)

C         Compute Darcy velocity

        IF (I .LT. NNODES) THEN
          DARVEL(I+1) = -(PERMEA(I+1)/VISLIQ(I))*((FLUPRE(I+1) -
     +         FLUPRE(I))/DELZ - DENLIQ*(-1.0D+00*GRAVAC))
        END IF

  110   CONTINUE
      DARVEL(1) = DARVEL(2)
```

```
C     Check to see if wave flux-related data should be sent to time output file

      IF ((TIMSTP .LE. NMTOUT) .OR. (MOD(N,TPRIVL) .EQ. 0) .OR.
     +    (N .EQ. TIMSTP) .OR. (N .EQ. 1)) THEN

C     Find bottom of wave by comparing current fluid pressure to
C     background fluid pressure

        I=1

 120    IF ((FLUPRE(I) - BKGPRE(I)) .GT. 0) THEN
          WAVBOT = Z(I)
          IBOT = I
        ELSE
          I=I+1
          GO TO 120
        END IF

C     Find peak of wave by locating maximum fluid pressure

        MAXPRE = FLUPRE(I) - BKGPRE(I)

 130    IF ((FLUPRE(I) - BKGPRE(I)) .LT. MAXPRE) THEN
          WAVEPK(2) = Z(I-1)
          IPK = I-1
        ELSE
          MAXPRE = FLUPRE(I) - BKGPRE(I)
          I=I+1
          GO TO 130
        END IF

C     Find top of wave by comparing current fluid pressure to background
C     fluid pressure:  top defined by location where fluid pressure is
C     less than 0.1% greater than the background fluid pressure

 140    IF (FLUPRE(I) .LT. 1.001D+00*BKGPRE(I)) THEN
          WAVTOP = Z(I)
          ITOP = I
        ELSE
          I=I+1
          GO TO 140
        END IF

C     Compute wave length

        WAVLEN = ABS(WAVTOP - WAVBOT)

C     Compute wave volume, assuming spherical geometry
```

```
      WAVVOL = (4.0D+00/3.0D+00)*PI*(WAVLEN/2.0D+00)**3

C     Compute the weighted average porosity of the wave

      PORSUM = 0.0D+00

      DO I = IBOT, ITOP
        PORSUM = PORSUM + POROS(I)*(Z(I) - Z(I-1))
      END DO

      WAVPOR = PORSUM/WAVLEN

C     Compute the wave pore volume

      WVPVOL = WAVVOL*WAVPOR

C     Compute wave velocity

      IF (N .GE. 2) THEN
        WAVVEL = (WAVEPK(2) - WAVEPK(1))/(TPRIVL*DELT)
      ELSE
        WAVVEL = 0.0D+00
      END IF

C     Set current wave peak location to old wave peak location

      WAVEPK(1) = WAVEPK(2)

C     Compute the length of time needed for the wave to traverse its
C     wavelength

      WAVTIM = WAVLEN/WAVVEL

C     Compute volumetric flow rate of wave

      WAVVFL = WVPVOL/WAVTIM

C     Write flux-related data to time output file

      WRITE(13,60) TIME, WAVBOT, WAVTOP, WAVEPK(2),
     +    WAVVEL*3.1536D+07, WAVLEN, WAVPOR, WVPVOL,
     +    WAVVFL*3.1536D+07

      END IF

C     Check to see if results should be printed to nodal output file
```

```
      IF ((N .EQ. PRTSTP(1)) .OR. (N .EQ. PRTSTP(2)) .OR. (N .EQ.
     +    PRTSTP(3)) .OR. (N .EQ. PRTSTP(4)) .OR. (N .EQ. PRTSTP(5))
     +    .OR. (N .EQ. PRTSTP(6)) .OR. (N .EQ. PRTSTP(7)) .OR.
     +    (N .EQ. PRTSTP(8)) .OR. (N .EQ. PRTSTP(9)) .OR.
     +    (N .EQ. PRTSTP(10))) THEN

        CALL TECWRT(Z, DEPTH, FLUPRE, TIME, NNODES, DARVEL, PERMEA,
     +      EFFSTR, POROS, SPECST, TEMP, VISLIQ, DENBLK)

      ENDIF

C         Report simulation progress at 5% increments

      SIMPRO = TIMSTP/20

      IF (MOD(N,SIMPRO) .EQ. 0) THEN
        WRITE(*,30) ' Timestep', N, 'completed.  Simulation',
     +      100*N/TIMSTP, '% done.'
      ENDIF

  500 CONTINUE

      STOP
      END

      SUBROUTINE TRIDIA(A, B, C, F, N, X)

C         This is the Thomas algorithm solution for tri-diagonal matrices given by Wang &
Anderson (1982)

      INTEGER N, NU, P1

      PARAMETER (P1=1000000)

      DOUBLE PRECISION A(P1), B(P1), C(P1), X(P1), F(P1), ALPHA(P1),

     +                 BETA(P1), Y(P1)

      ALPHA(1) = B(1)
      BETA(1) = C(1)/ALPHA(1)
      Y(1) = F(1)/ALPHA(1)

      DO I=2, N
        ALPHA(I) = B(I) - A(I)*BETA(I-1)
        BETA(I) = C(I)/ALPHA(I)
        Y(I) = (F(I) - A(I)*Y(I-1))/ALPHA(I)
      END DO
```

```
C       Begin backward substitution from last row

        X(N) = Y(N)
        NU = N-1
        DO I=1, NU
          J = N-I
          X(J) = Y(J) - BETA(J)*X(J+1)
        END DO

        RETURN
        END

      SUBROUTINE TECWRT(Z, DEPTH, FLUPRE, TIME, NNODES, DARVEL, PERMEA,
     +   EFFSTR, POROS, SPECST, TEMP, VISLIQ, DENBLK)

C     Subroutine to write results to TECPLOT-formatted output file

      INTEGER NNODES, P1

      PARAMETER (P1=1000000)

      DOUBLE PRECISION Z(P1), DEPTH(P1), FLUPRE(P1), TIME, DARVEL(P1),
     +   PERMEA(P1), EFFSTR(P1), POROS(P1), SPECST(P1), TEMP(P1),
     +   VISLIQ(P1), DENBLK(P1)

   10 FORMAT(A13, E8.3, 1X, A7, 1X, A4, I6, A2)
   20 FORMAT(11(E15.5,2X))

      WRITE(12,10) 'ZONE T = "', TIME, 'years",', 'I = ', NNODES

      DO I = 1, NNODES

        WRITE(12,20) Z(I),DEPTH(I), FLUPRE(I)/1.0D+06,
     +   DARVEL(I)*3.1536D+07, PERMEA(I), EFFSTR(I)/1.0D+06,
     +     POROS(I)*100., SPECST(I), TEMP(I), VISLIQ(I), DENBLK(I)

      END DO

      RETURN
      END
```